Macroscopic quantum coherence phenomena in Bose Einstein Condensates

Stefano Giovanazzi

September 23, 1998

Contents

Chapter 1

Introduction

The recent experimental observation [1, 2, 3, 4, 5] of Bose-Einstein Condensation (BEC) in dilute Bose gas of alkali atoms can be considered a milestone in the history of the BEC. For the first time, evidences of the BEC, have been obtained in simple and direct ways. Vapors of rubidium and sodium were confined in magnetic (harmonic) traps and cooled down to temperatures of the order of the nanokelvin. Below the critical temperature a sharp peak in the velocity distribution was observed, after switching off the confining potential [6]. Such anisotropic velocity distribution cannot be interpreted as a thermal distribution, providing therefore a clear signature of BEC.

The peculiarity of these trapped alkali vapors is that their densities are sufficiently low so that such gases can be realistically treated in the framework of the theory of the weakly interacting Bose gas, which is well established. At the same time the interaction is effective on many relevant properties of the system and its strength is sufficient to allow for the condensation in a finite time. This feature makes the Bose Einstein condensation not only very interesting, from an experimental point of view, but also a very challenging theoretical problem.

A very attractive aspect, from the theoretical point of view, is that alkali

vapors are inhomogeneous and interacting systems. In fact, a very complex and rich phenomenology is expected, as a consequence of the interplay between inhomogeneity and interaction. For example, the shape and the spatial extension of the trapped condensate can be strongly modified by the two body interaction[1]

A striking feature of a BEC is its coherent nature, which is related to the *macroscopic quantum phase* of the system. An important consequence of this is the possibility of interference phenomena. Such phenomena have been already observed in dilute alkali condensates, proving the coherent nature of these systems over a macroscopic scale. In a beautiful experiment, performed at MIT [7], two *independent* condensates were created in a double well potential, obtained by focusing a off-resonant laser light into the center of the magnetic trap. After switching off the confining potential and the laser, the Bose Einstein condensates expanded and successively overlapped. Clean atomic interference patterns have been observed in the overlapping region.

Recently the JILA group [8], using an interferometric technique, has measured the relative phase between two trapped condensates in different hyperfine states and its subsequent time-evolution. Contrary to the MIT experiment [7], the initial state is, from the beginning, a coherent superposition of two condensates; the JILA group was also able to show that each realization of the experiment reproduces the same evolution for the relative phase.

A classical experiment that investigates the role of the macroscopic quantum phase difference on the evolution of two coupled macroscopic quantum systems is the Josephson-junction experiment. The Josephson experiment represents the usual way to detect the phase of the order parameter in superconductors, through the observation of coherent oscillations of Cooper-pairs. In the context of alkali gases an advantage of the Josephson experiment is that, differing from the interference experiment, it does not destroy the sample. In particular, Josephson experiment allows for a continuous measurement of the phase difference, through the monitoring of the population difference, e.g. by phase-contrast microscopy [9].

Arguments first proposed over thirty year ago by Josephson, Anderson and Feynman [10, 11, 12], based on fundamental quantum-mechanical principles, lead to the prediction that if two macroscopic quantum systems are weakly cou-

[1]The spatial extension of the condensate can be orders of magnitude bigger than that of the ideal condensate gas.

pled together, particle currents should oscillate between the two systems. If the two systems have a quantum phase difference, a supercurrent must flow from one system to the other. The current I is related to the phase difference $\Delta\phi$ by the equation $I = I_c \sin(\Delta\phi)$, where I_c is the critical current of the link. If the two systems have a chemical potential difference $\Delta\mu$, the phase difference evolves with time t according to the equation $\partial(\Delta\phi)/\partial t = -\Delta\mu/\hbar$.

Josephson effects have been searched experimentally in weak links between neutral superfluid systems, such as ^{4}He-2 and ^{3}He-B (systems of bosons and fermions respectively). Only very recently it has been observed an oscillating mass current in a weak link between two superfluid ^{3}He-B reservoirs [13, 14, 15].

The main subject of this thesis are Josephson-like effects in a weak link between two trapped alkali BEC gases. The time rate of change of the relative population, is the BEC analog of the supercurrent in the usual Superconductor Josephson Junction (SJJ). The interest in this system arises from the expectation of new dynamical regimes, which are not experimentally accessible in SJJ, since macroscopic changes in density are forbidden for a SJJ. A further motivation to investigate this system comes from the absence of noise due to external experimental apparatus. For instance, in a SJJ the external electrical circuits is a source of noise.

The Josephson dynamics between two weakly linked BECs of alkali gases has been already a source of several theoretical investigations [16, 17, 18, 19, 20, 21, 22]. At least two different experiments can be suggested in order to obtain a weak link between two BECs of alkali gases. In a setup similar to that of MIT, one can imagine to lower the width of the laser to allow coupling between the condensates; the coupling arises from quantum tunneling [17]. This kind of setup will be the object of a detailed discussion in chapter 4. A different kind of weak link can be obtained by considering two trapped condensates in different hyperfine states, like that proposed by JILA group [22]. In this case the role of tunneling is played by a weak driving field that couples these hyperfine states.

An other important reason to study BEC of alkali gases is that the system can be realistically described, at low temperature, by the theory of weakly interacting Bose gas, as developed by E. Gross and L. Pitaevskii [23]. The mean field analysis, for alkali BECs, provides an accurate realistic description of the

non-linear dynamics and provides a simple language to understand the system in terms of few physical quantities. At zero temperature the condensate is described by a *one-body wave function* and its time evolution satisfies a non linear Schrödinger equation (the Gross-Pitaevskii equation). In the inhomogeneous case the exact solution of this equation requires a numerical approach that will be the object of Chapters 5 and 7.

In the physics of SJJ, the low energy dynamical behaviour is well described, both phenomenologically and microscopically, in terms of the current I and the phase difference ϕ between the two superconductors. In a similar way, in neutral superfluid systems, as ^{4}He-2 and ^{3}He-B, the low energy dynamical behaviour is described in terms of an effective free energy $F(\phi, \delta N)$, where the relative phase ϕ and the relative number δN can be treated as canonically conjugate variables.

Our starting point has been to extend the SJJ language to the case of weakly linked BECs. The approach used for this reason is the time dependent variational approximation (or Dirac action principle) applied to the full mean field equation (chapter 4). In our variational Ansatz the order parameter is written as a superposition of two time-independent wave functions. In such a way a formal description in terms of the relative phase ϕ and the relative number δN can be obtained. These variables are canonically conjugate and satisfy two coupled non linear equations (that we refer to TMA) in terms of few static properties, that in some limit can identified as the Josephson coupling energy, and the Josephson capacitative energy.

Such approach has enabled the investigation of interesting non linear effects. We have found that new effects can arise due to the interaction and/or to the particular initial condition of the BECs. One of these is the so called self-locked population imbalance: for instance, in the case of a double well symmetric potential, two condensates, prepared with an initial imbalance above a critical value, cannot evolve with a dynamics with zero average population imbalance, but the population of the two states make small and fast oscillations near the initial condition. This effect is analogous to the AC effect observed in SJJ.

In TMA equations the dynamics depends, a part from a time scale factor, only on the ratio of the Josephson capacitative energy and the Josephson coupling energy. If this ratio is very large, a behaviour similar to the SJJ is observed;

if the ratio is close to zero, Rabi-like oscillations are obtained.

Another important result, obtained by TMA equations, is that under certain circumstances, a quantum phase difference of π between the two trapped Bose gas, can be maintained. This will be discussed in chapter 4. Very recently, a similar phenomena, was observed in a weak link between two superfluid ^{3}He-B reservoirs [24].

In chapter 5 we have gone beyond the TMA by integrating the full GPE. There are at least two important reasons to do this: first, to check the limit of validity of the TMA, second, to look for new effects, which cannot be described by the TMA, as, for instance, the relaxation phenomena. Furthermore, in a very inhomogeneous Bose gas, we expect that non trivial effects can occur, due to the coupling between intrawell collective motions and interwell Josephson dynamics.

The results obtained by the full integration of GPE can be used to develope an "effective" TMA, as we will show in chapters 5 and 7. In this approach the Josephson coupling energy and the Josephson capacitative energy, appearing in the TMA equations, are treated as "phenomenological" inputs. An effective description of the numerical results in terms of the formal equations of the TMA model is obtained [25].

These numerical methods (second part of chapter 4) can provide the experimentalists with accurate values for the laser parameters that should be used in order to observe these effects.

An open problem is the actual experimental observation of Josephson oscillations as well as the measure of both the plasma frequency and the critical current. One of the limiting factors is that the amplitude of Josephson oscillations can be too low for the present resolution of the available experimental setups[2]. In chapter 7 it will be proposed a strategy to improve the observability of Josephson-like effects. This strategy leads to a measure of the critical current and the Josephson frequency, even in the case in which the Josephson oscillations cannot be directly observed [26]. We suggest to investigate experimentally a phenomenon that is the close analog of what occurs in a single SJJ under the action of an external dc current source. The dc $I-V$ curve, $V=V\left(I\right)$, can be explored and the analog of the dc and ac effects can be formally recovered. The

[2]The frequency of Josephson oscillations can be a fraction not neccessarily small of those of the trap.

role of the external electric circuits with a current source is played by a slow relative motion of trapping potential with respect to the laser sheet, where the relative velocity corresponds to the intensity of the external applied current in SJJ. The existence of the critical current manifest itself in the occurrence of a critical value of the relative velocity.

Chapter 2

Bose-Einstein Condensation

2.1 Bose-Einstein Condensation in dilute trapped alkali gas

The Bose-Einstein condensation (BEC) has been the source for several studies and debates, leading to the development of continuously novel technics for the investigation of different physical systems [27]. In this context, the recent experimental observation of Bose-Einstein condensation, in dilute Bose gas of alkali atoms [1, 2, 3, 4, 5], has to be considered as fundamental achievement.

Previous investigations of BEC have been mostly limited to superfluid ^{4}He, namely liquid ^{4}He below the critical temperature ($T_c = 2.3\ ^oK$) [28]. Since early stages, superfluidity was considered as a manifestation of BEC. This is an issue which is still very much debated. Then, some more direct observations of BEC came from the deep inelastic neutron scattering experiments on ^{4}He, which, at high momentum transfer, provide a measure of the momentum distribution $n\left(k\right)$ [29]. The Bose condensate should appear as a delta function singularity of $n\left(k\right)$ at $k = 0$. However, due to final state interactions of the knock out atom with the

bulk and to experimental broadening effects, the delta function is not directly observable. Making use of theoretical models, based on microscopic calculations [30], the fraction of Bose condensation in ^{4}He has been estimated to be 7.3%. Therefore, due to the strong short-range correlations the fraction of the condensate is very small. This makes very difficult to quantitatively study the dynamical behaviour of such condensate, both experimentally and theoretically. Other investigations of the BEC properties have been done in other many-body systems, such as the gas of excitons in semiconductor [31], the pairs in superconductor materials and the superfluid ^{3}He.

The remarkable experiments leading to Bose-Einstein condensation in alkali gas have been performed by combining sophisticated non linear optical techniques. Atoms were confined in harmonically magneto-optical traps and cooled down with laser cooling and evaporative cooling techniques [32]. In this way it has been possible to reach the temperature and density values necessary to observe the phenomenon of Bose-Einstein condensation[1]. In this conditions the equilibrium configuration of the system would be the solid phase. Since three-body collisions are rare events in dilute and cooled gases, the metastable gas phase has a sufficiently long lifetime[2] and the BEC can be observed. The first evidence for condensation emerged from the free expansion of the condensate after switching off the confining trap: a sharp peak in the velocity distribution appeared below a critical temperature.

The dilute nature of these gas allows one to describe the two body interaction with a single parameter, the s-wave scattering length (Born approximation). The static and dynamical properties of the Bose-Einstein condensate can be realistically studied within the theory of weakly interacting Bose gas, mainly developed by Gross and Pitaevskii [23] (see next section). Standard methods, used for homogeneous dilute Bose gas, have been extended to the inhomogeneous and finite number of atoms case, and new techniques have been developed to investigate static and dynamics properties of the BEC, as well as its temperature dependence [**?**].

Condensate alkali atoms constitute a nearly ideal system (condensate frac-

[1]For a homogeneous gas the condition for BEC is $(\lambda_{DB})^3 \rho > 2.612$, where $\lambda_{DB} = \frac{\hbar}{mk_B T}$ is the De Broglie wave length and ρ is the density of the systems.

[2]The observed lifetime of the condensate depends also on other different scattering mechanisms with incoherent photons and impurity atoms.

Figure 2.1: The MIT condensate.

tion $\sim 100\%$), in which short-range correlations can be neglected and the mutual interaction can be treated in Ψ^4 theory (mean field theory). Despite such systems can be considered as a weakly interacting Bose gas, one should not have the impression that, the two body interaction plays a minor role. In fact, the interaction, in addition to be crucial for the actual realization of BEC[3], it is also very effective on various of their relevant properties [4]. For instance, the non linear effects, due to two body interactions, raise the most important physical problems in this field of research.

[3]The intensity of the interaction gives the rate of termalization processes.
[4]such as the spatial extension of the BEC and non linear dynamical effects

Bose-Einstein condensation in alkali gas is quickly developing as a broad interdisciplinary field, where concepts coming from different areas of physics, such as quantum optics, statistical mechanics and condensed matter physics, can be encountered. Among the several theoretical perspectives, in this thesis we will focus on the non linear dynamics behaviour of the condensate and its coherence effects at zero temperature.

We will limit ourself to a mean-field description of the behaviour of these systems, which is adequate enough, given the accuracy of the present experimental data. This theory has been already tested with excellent success in the description of various fundamental properties of these systems in different physical regimes [**?**]. It can also be the starting point for the investigation of novel phenomena.

This chapter will introduce the Gross-Pitaevskii equation, the Thomas-Fermi approximation, the Bogoliubov theory for the collective excitations and the non linear dynamical aspects for BEC.

2.2 The Gross-Pitaevskii Theory

The theory of the condensate of a weakly interacting Bose gas was developed by E. P. Gross and L. L. Pitaevskii [23]. Although Gross-Pitaevskii and Bogoliubov [33] theories are not realistic theories to study the physical properties of ^{4}He at low temperature, they are very well suited for condensed low density alkali gas. Such theories have been generalized to the inhomogeneous case [34], as needed for trapped condensates.

The problem of N interacting bosons is in general a very complicated one. The dynamical evolution of the systems is described by a N body wave function. In the case of a weakly interacting Bose gas, however, strong simplifications occur in the description of the system under the occurrence of the BEC phenomenon. In fact, the system is sufficiently dilute, the interaction potential fulfils the conditions of applicability of Born approximation, and it can be represented by a $g\left|\Psi\right|^4$ term, where the coupling constant g is directly related to the s-wave scattering length. The condensate is described by a *"one body"* wave function normalized to the number of particles [5] (of the condensate). The collec-

[5] in chapters 4,5,6 we use another choice of normalization associated with a particular choice of unit

tive dynamics of a dilute Bose gas at zero temperature is therefore described by a *"macroscopic wave function"* $\Psi(\mathbf{r},t)$, which obeys a nonlinear Schrödinger, or Gross-Pitaevskii equation (GPE) [23]:

$$i\hbar\frac{\partial}{\partial t}\Psi\left(\mathbf{r},t\right) = -\frac{\hbar^2}{2m}\boldsymbol{\nabla}^2\Psi\left(\mathbf{r},t\right) + \left[V_{ext}\left(\mathbf{r},t\right) + g\left|\Psi\left(\mathbf{r},t\right)\right|^2\right]\Psi\left(\mathbf{r},t\right) \qquad (2.1)$$

where $V_{ext}\left(\mathbf{r},t\right)$ is the external confining potential and the coupling constant g is given by $g = 4\pi\hbar^2 a/m$, where a is the atomic s-wave scattering length and m the atomic mass. In this non linear Schrödinger equation, the non linearity comes from the interaction in the form of a self-consistent field $g\left|\Psi(\mathbf{r})\right|^2$. The static (ground state) solution obeys the GP equation

$$-\frac{\hbar^2}{2m}\boldsymbol{\nabla}^2\Psi\left(\mathbf{r}\right) + \left[V_{ext}\left(\mathbf{r}\right) + g\left|\Psi\left(\mathbf{r}\right)\right|^2\right]\Psi\left(\mathbf{r}\right) = \mu\,\Psi\left(\mathbf{r}\right) \ . \qquad (2.2)$$

where the eigenvalue μ is the chemical potential $\mu = E\left(N\right) - E\left(N-1\right)$.

The main feature of eq.s. 2.1 and 2.2 is the competition between the kinetic energy and the mean field. One limiting case is to neglect the kinetic energy in eq. 2.2. This correspond to the Thomas-Fermi approximation; in such approximation the static solution is given by

$$\Psi\left(\mathbf{r}\right) = \frac{1}{\sqrt{g}}\sqrt{\mu - V_{ext}\left(\mathbf{r}\right)}\Theta\left(\mu - V_{ext}\left(\mathbf{r}\right)\right) \ , \qquad (2.3)$$

(where Θ is the unit step function). The Thomas-Fermi approximation can be used when the mean field is much bigger than the kinetic energy and it is a particularly suited to analyze the effect of the interactions. The Thomas-Fermi approximation leads to a rather simplified treatment of the low energy dynamical behaviour[6] [35].

The effect of the interaction term $g\left|\Psi\right|^2$ can lead to drastic changes in static and also dynamics properties of the BEC. The shape and in particular the spatial size of the condensate can change significantly with respect to the non interacting ground state (gaussian shaped). This effect is particularly large when the Thomas-Fermi approximation is valid, as can be seen from eq. 2.3. Since the stationary solution of 2.2 follows from a variational principle, virial relations can be obtained. One of these relations is the following

$$T_x - V_x^{ho} + \frac{1}{2}U_{int} = 0 \ , \qquad (2.4)$$

length: $\int d\mathbf{r}\ |\Psi|^2 = 1$, and consequently $g \to Ng$, where N is the number of condensate atoms.

[6] this treatment in some cases leads to analitycal solutions

where $T_x = \langle -\frac{\hbar^2}{2m}\frac{\partial^2}{\partial x^2}\rangle$ and $V_x^{ho} = \langle \frac{1}{2}m\omega_x^2 x^2\rangle$ are the kinetic energy and the harmonic potential energy corresponding to the x axis, and $U_{int} = \langle \frac{1}{2}g\left|\Psi\right|^2\rangle$ is the internal energy (two similar equations hold for the y and z components).

In the following we sketch one of the possible derivation of the GPE. In the formalism of second quantization, a system of N interacting bosons of mass m, interacting through a two body potential V and confined by an external potential V_{ext}, is described by the following general Hamiltonian:

$$\begin{aligned} H &= \frac{\hbar^2}{2m}\int \nabla\hat{\Psi}^\dagger\nabla\hat{\Psi} + \int V_{ext}\left(\mathbf{r}\right)\hat{\Psi}^\dagger\hat{\Psi} \\ &\quad + \frac{1}{2}\int \hat{\Psi}^\dagger\left(\mathbf{r}\right)\hat{\Psi}^\dagger\left(\mathbf{r}'\right)V_{int}\left(\mathbf{r}-\mathbf{r}'\right)\hat{\Psi}\left(\mathbf{r}\right)\hat{\Psi}\left(\mathbf{r}'\right)d\mathbf{r}'\,d\mathbf{r}\,, \end{aligned} \tag{2.5}$$

where $\hat{\Psi}^\dagger\left(\mathbf{r}\right)$, $\hat{\Psi}\left(\mathbf{r}\right)$ are field operators satisfying the Bose commutation rules

$$\left[\hat{\Psi}^\dagger\left(\mathbf{r}\right),\hat{\Psi}\left(\mathbf{r}'\right)\right] = \delta\left(\mathbf{r}-\mathbf{r}'\right),\ \left[\hat{\Psi}\left(\mathbf{r}\right),\hat{\Psi}\left(\mathbf{r}'\right)\right] = 0,\ \left[\hat{\Psi}^\dagger\left(\mathbf{r}\right),\hat{\Psi}^\dagger\left(\mathbf{r}'\right)\right] = 0. \tag{2.6}$$

The dynamics follow from the Heisenberg equation of motion for the time dependent operators $\hat{\Psi}^\dagger\left(\mathbf{r},t\right)$, $\hat{\Psi}\left(\mathbf{r},t\right)$

$$i\hbar\frac{\partial}{\partial t}\hat{\Psi}\left(\mathbf{r},t\right) = \left[\begin{array}{c} -\frac{\hbar^2}{2m}\nabla^2 + V_{ext}\left(\mathbf{r}\right) \\ +\int \hat{\Psi}^\dagger\left(\mathbf{r}',t\right)V_{int}\left(\mathbf{r}-\mathbf{r}'\right)\hat{\Psi}\left(\mathbf{r}',t\right)d\mathbf{r}' \end{array}\right]\hat{\Psi}\left(\mathbf{r},t\right) \tag{2.7}$$

If the interaction potential $V_{int}\left(\mathbf{r}-\mathbf{r}'\right)$ fulfils the conditions of applicability of the Born approximation, then it can be substituted by an effective contact interaction $a\cdot\delta\left(\mathbf{r}-\mathbf{r}'\right)$ where a is proportional to the scattering length; this is also equivalent to neglect short range correlations. The Gross-Pitaevskii equation (GPE) follows from the semiclassical theory obtained by replacing the commutation rules for $\hat{\Psi}^\dagger\left(\mathbf{r}\right)$, $\hat{\Psi}\left(\mathbf{r}\right)$ with classical Poisson Bracket relations. The Heisenberg equation of motion becomes a non linear integrodifferential equation governing a classical field.

An alternative derivation of GPE follows from the Bogoliubov prescription, in which the field operator is shifted by a c-number $\Phi\left(\mathbf{r},t\right)$

$$\hat{\Psi}\left(\mathbf{r},t\right) = \Phi\left(\mathbf{r},t\right) + \hat{\Psi}'\left(\mathbf{r},t\right)\,, \tag{2.8}$$

where $\Phi\left(\mathbf{r},t\right)$ is a scalar complex function defined as the expectation value of the field operator in the Gran canonical ensemble $\Phi\left(\mathbf{r},t\right) = \langle\hat{\Psi}\left(\mathbf{r},t\right)\rangle$. The function $\Phi\left(\mathbf{r},t\right)$ has the physical meaning of an order parameter and it is also called *"condensate wave function"*, emphasizing the existence of a macroscopic number of

bosons in the condensate. It is possible to obtain the equation for the condensate wave function, namely the GPE, by replacing in the Heisenberg equation of motion 2.7 the field operator $\hat{\Psi}(\mathbf{r},t)$ with the expression in the eq. 2.8 and requiring that the first order in $\hat{\Psi}'(\mathbf{r},t)$ is identically zero.

In an inhomogeneous and finite system the condensate wave function has the following clear meaning: it can be determined through the diagonalization of the one-body density matrix $\langle \hat{\Psi}^{\dagger}\left(\mathbf{r}^{'},t\right),\hat{\Psi}(\mathbf{r},t)\rangle$ and corresponds to the eigenfunction with the largest eigenvalue, namely directly related to the condensate fraction n_0 [36].

2.2.1 Linearized GPE or Bogoliubov approximation

An appropriate description of the low energy elementary excitations at zero temperature in the condensate alkali gas can be obtained from the GPE. Elementary excitations can be viewed as small oscillations around the ground state. Their frequency can then be obtained by linearizing the GPE. To this purpose we write $\Psi(\mathbf{r},t)$ in the form of

$$\Psi(\mathbf{r},t)=\exp\left(-i\mu_0 t/\hbar\right)\left[\Psi_0(\mathbf{r})+\delta\Psi(\mathbf{r},t)\right]. \tag{2.9}$$

This is still a solution of the GPE to first order in $\delta\Psi$ if $\delta\Psi$ satisfies the equation

$$\begin{aligned} i\hbar\frac{\partial}{\partial t}\delta\Psi(\mathbf{r},t) = - & \quad \frac{\hbar^2}{2m}\boldsymbol{\nabla}^2\Psi(\mathbf{r},t)+\left(V_{ext}(\mathbf{r})-\mu_0\right)\delta\Psi(\mathbf{r},t) \\ & +2g\left|\Psi_0(\mathbf{r})\right|^2\delta\Psi(\mathbf{r},t)+g\left|\Psi_0(\mathbf{r})\right|^2\delta\Psi^*(\mathbf{r},t)\ . \end{aligned} \tag{2.10}$$

The solution of this equation can be written in the form

$$\delta\Psi(\mathbf{r},t)=u(\mathbf{r})\exp\left(-i\omega t\right)-v^*(\mathbf{r})\exp\left(+i\omega t\right), \tag{2.11}$$

and equation 2.10 becomes

$$\begin{aligned} \hbar\omega\, u(\mathbf{r}) &= \left[H_0-\mu_0+2g\left|\Psi_0(\mathbf{r})\right|^2\right]u(\mathbf{r})-g\left|\Psi_0(\mathbf{r})\right|^2 v(\mathbf{r})\ , \\ -\hbar\omega\, v(\mathbf{r}) &= \left[H_0-\mu_0+2g\left|\Psi_0(\mathbf{r})\right|^2\right]v(\mathbf{r})-g\left|\Psi_0(\mathbf{r})\right|^2 u(\mathbf{r})\ , \end{aligned} \tag{2.12}$$

where $H_0=-\left(\hbar^2/2m\right)\boldsymbol{\nabla}^2+V_{ext}(\mathbf{r})$. The energy ϵ associated to each elementary excitations corresponds to the frequency ω of the relative small oscillations around the ground state

$$\epsilon=\hbar\omega\ . \tag{2.13}$$

This procedure is equivalent to the diagonalization of the many body Hamiltonian in the Bogoliubov approximation. For most recent reviews see A. Fetter [34], and Gardiner [37].

2.2.2 non linear dynamics

In order to study the non-linear dynamics of finite size systems one needs to numerically integrate the GPE. Based on the experimental results or on the numerical solutions, one can try to find approximate solutions for such dynamics, that may lead to a more intuitive picture of the system properties. To this aim a powerful approach is the time dependent variational principle. This approach applied to the collective motions leads to an excellent determination of their frequency [38].

Chapter 3

Aim and plan of the work

3.1 The weak link between two BECs

A striking feature of a Bose Einstein Condensate is its coherent nature. An important consequence of this is the possibility of interference phenomena. Such phenomena have been already observed in a dilute alkali condensates, proving the coherent nature of these systems over a macroscopic scale. In this beautiful experiment, performed at MIT [7], two condensates were created in a double well potential, obtained by focusing a blue-detuned far-off-resonant laser light into the center of the magnetic trap. After switching off the confining potential and the laser, the Bose Einstein condensates expanded and successively overlapped. Clean atomic interference patterns have been observed in the overlapping region (see fig. 3.1).

It is important to stress that this interference phenomenon was observed between two *independent* Bose Einstein Condensates. This experiment should be considered as equivalent to the Anderson's gedanken experiment ("What is the relative phase of two buckets of liquid helium") [11] and also to the interference experiment between two independent sources of coherent light [39] (a remark-

Figure 3.1: A striking feature of a Bose Einstein Condensate is its coherent nature. The first evidence, that clearly proves phase coherence over a macroscopic scale in dilute alkali condensate, have been obtained through the observation of interference phenomena. Two *independent* Bose Einstein Condensates were obtained in a double well potential in a recent experiment at MIT [7].Switching off the confining potential, the condensates expanded and successively overlapped. Clean atomic interference patterns have been observed in the overlapping region.

able experiment in non linear optics, that disproved a famous statement of Dirac [40] "...each photon interferes only with itself. Interference between different photons never occurs.").

Recently the JILA group [8] using an interferometric technique have measured the relative phase between two trapped condensates in different hyperfine states and its subsequent time-evolution. A Condensate of ^{87}Rb atoms, initially in the $|f = 1, m_f = -1\rangle$ hyperfine state, is driven, through a two-photon transition. After a $\pi/2$ pulse the condensate becomes a superposition of the two hyperfine states, $|f = 1, m_f = -1\rangle$ and $|f = 1, m_f = 1\rangle$, with equal population. Contrary to the MIT experiment [7], the initial state is, from the beginning, a co-

herent superposition of two condensates; the JILA group was also able to show that each realization of the experiment reproduces the same evolution for the relative phase.

A classical experiment that investigates the role of the *macroscopic quantum phase (difference)* on the evolution of two coupled macroscopic quantum systems is the Josephson-junction experiment. The Josephson experiment represents the usual way to detect the phase of the order parameter in superconductors, through the observation of coherent oscillations of Cooper-pairs. There have been several proposals [16, 17, 18, 19, 20, 21] suggesting an analogous experiment in the context of BEC of trapped alkali gases. In a setup similar to that of MIT, one can imagine to lower the intensity of the laser (or/and its width if it is possible) to allow coupling between condensates arising from quantum tunneling. One could observe the time rate of change of the relative population, which is the analog of the supercurrent in the usual Superconductor Josephson Junction (SJJ). This should enable the investigation of interesting non linear effects, due to two-body interaction.

A different type of weak link experiment, based on the work, done by the JILA group [8], with two trapped condensates in different hyperfine states, has also been recently proposed [22], in which, the role of tunneling is substituted by a weak driving field that couples these internal states [1].

Both the two weak-link BEC experiments proposed (the first with a double-well potential created by a laser sheet, and the second using a two component condensates coupled by a driving field) have the lifetime of the condensate as a possible experimental limitation. We assume in the following that the lifetime of the condensate is sufficiently long so that macroscopic quantum tunneling phenomena can be observed.

The Josephson effects and related features which can be explored with a trapped Bose gas, has been theoretically studied, within the so called two mode approximation, in a number of recent papers [16, 17, 18, 19, 20, 21, 25, 26]. In this thesis, we investigate the occurrence of Josephson like effects in a weak link between two trapped BECs. The principal part of this work is directly related to the double potential case.

The Mean field Theory is a powerful tool to qualitatively and quantitatively

[1] (with a Rabi period longer than the typical time scale of internal motions)

understand the dynamical behaviour of the Condensate. The Gross-Pitaevskii theory is in a good quantitative agreement with the data from interference experiments. This is very important because it reveals that the concept of phase coherence, as assumed in GP theory, is a very sound one, and suggests that it can be a remarkable starting point to investigate Josephson like effects in weak links. However, it is not a priori obvious that GP theory provides good quantitative description of the weak link physics. It is then imperative to test quantitatively such mean field theory and check whether it can be considered as a basis for more sophisticate treatments.

Assuming that the GP mean field is appropriate, We will compare the physics of SJJ and TMA, looking for dynamical regimes not observable in SJJ. These are the main goals of this work.

In the physics of Superconductor Josephson Junction, the low energy dynamical behaviour is well described (both phenomenologically and microscopically) in terms of the current I and the phase difference ϕ between two superconductors. Since a long time Josephson like effects have been theoretically predicted in a weak link between superfluids as ^{4}He-2 and ^{3}He-B. In such neutral systems the low energy dynamical behaviour is described in terms of an effective free energy $F(\phi, \delta N)$, where the relative phase ϕ and the relative number δN can be treated as canonically conjugate variables. It is only recently that Josephson like effects have been explicitly observed experimentally in a weak link between two superfluid ^{3}He-B reservoir [13, 14, 15].

Our starting point is to establish such language in the context of weak links in condensation of alkali atoms. The simplest and still realistic scheme that we have used is the Two Mode Approximation (TMA) model, which is based on the Dirac action principle [41], or time dependent variational method. The approximate initial Ansatz is that the order parameter is written as a superposition of two static spatial dependent wave functions. In such a way a formal description in terms of the relative phase ϕ and the relative number δN can be obtained. These variables are canonically conjugate and satisfy two coupled non linear equations in terms of few static properties. One should underline that the problem of finding good variational time independent wave function is not at all trivial.

It is however necessary to go beyond the TMA and to investigate the full

GPE for at least two important reasons:

- 1) a comparison with the TMA to check its limit of applications;
- 2) the occurrence of possible new effects, not present in the TMA, as for instance the damping. In fact, in such inhomogeneous Bose gas, we expect that non trivial effects can occur, from the strong coupling between intrawell collective motions and interwell Josephson dynamics.

In section 2 the plan of the work is summarized, whereas the time dependent variational method and the numerical solution of GPE are briefly discussed in section 3.

3.2 Plan of the work

- A general analytical description of the non linear tunneling dynamics of a weak link between two trapped BECs within TMA (based to the time dependent variational principle).
- A comparison with SJJ and a search for new dynamical regimes.
- An analysis of a possible choice of the two effective order parameters, which is not based on the usual perturbation scheme.
- The full numerical integration of the Gross-Pitaevskii equations (which goes beyond the TMA).
- A comparison between the numerical results and those obtained in the TMA.
- An effective ”phenomenological” description of the numerical results in terms of the formal equations of the TMA model.
- The investigation of possible effects due to the coupling with interwell collective excitations.
- A search for the best geometry and experimental setup to observe Josephson like effects.

3.3 Methods

3.3.1 The Time-Dependent Variational Principle

Some general properties

Any variational approximation to the dynamics of a quantum system based on the Dirac action principle [41] leads to a classical Hamiltonian dynamics for the variational parameters. The starting point for a variational calculation is Dirac's action principle which can be used to derive the Gross-Pitaevskii equation as shown below. We begin by defining the Gross-Pitaevskii action functional (not normalized):

$$S = \int_1^2 dt \, \langle \, \Psi \, | \left(i\frac{\partial}{\partial t} - H - U \right) | \, \Psi \rangle \ , \tag{3.1}$$

where $H_0 = -\frac{\hbar^2}{2m}\boldsymbol{\nabla}^2 + V\left(\mathbf{r},t\right)$ and $U = \frac{1}{2}g\left|\Psi\left(\mathbf{r},t\right)\right|^2$. From the variational principle $\delta S = 0$, along with the boundary conditions $\delta|\,\Psi\left(t_1\right)\rangle = 0;\, \delta|\,\Psi\left(t_2\right)\rangle = 0$ we get

$$\delta S = 2\int_1^2 dt \ \mathrm{Re}\langle \, \delta\Psi \, | \, i\frac{\partial}{\partial t} - H - 2U \, | \, \Psi \rangle \, , \tag{3.2}$$

which leads (the variation $\langle \, \delta\Psi \, |$ is arbitrary) to the time-dependent GPE (or non-linear Schrödinger equation)

$$\left(i\frac{\partial}{\partial t} - H - 2U \right) | \, \Psi \rangle \ = 0 \ . \tag{3.3}$$

Most of the analytical studies are based on the variational method, in which the (approximate) solution $|\,\Psi_T\rangle$ is restricted to same trial manifolds. In this case the variation $|\delta\Psi\rangle$ is not fully arbitrary. The trial wave function is determined by a set of n time-dependent variational parameters of the form $q_i\left(t\right), i = 1, n,$ and written formally as

$$\Psi(\, x,\, t) = \Psi_T \left(\, x,\, q_i\left(t\right)\right) \ .$$

The action S calculated along the trial wave functions is given by

$$\begin{aligned} S_T\left[q\right] &= \int_1^2 dt \, \langle \, \Psi_T \, | \left(i\frac{\partial}{\partial t} - H - U \right) | \, \Psi_T \rangle \\ &= \int_1^2 dt \ L\left(q, \dot{q}\right) \, , \end{aligned}$$

where the Lagrangian L is always given by functions of the form,

$$L\left(q, \dot{q}\right) = \pi_i\left(q\right) \ \dot{q}_i - H\left(q\right) - U\left(q\right) \ ,$$

where

$$\pi_i(q) = i\langle \Psi_T \mid \frac{\partial \Psi_T}{\partial q_i}\rangle ,$$

Extremization of the action via $\delta S[q] = 0$ yields the dynamical equations obeyed by the variational parameters $q_i(t)$

$$M_{ij}(q)\ \dot{q}_j = \frac{\partial}{\partial q_i}\left(H(q) + U(q)\right) , \tag{3.4}$$

where M is an anti-symmetric matrix given by

$$\begin{aligned} M_{ij}(q) &= \frac{\partial \pi_i(q)}{\partial q_j} - \frac{\partial \pi_j(q)}{\partial q_i} , \\ &= 2\,\mathrm{Im}\langle \frac{\partial}{\partial q_j}\Psi_T \mid \frac{\partial}{\partial q_i}\Psi_T\rangle . \end{aligned}$$

If the inverse of M exists, the equations of motion can be written in the form:

$$\dot{q}_j = M^{-1}_{ji}(q)\frac{\partial}{\partial q_i}\left(H(q) + U(q)\right) .$$

Since M^{-1} is also antisymmetric, $H(q) + U(q)$ is a conserved quantity ($\dot{H} + \dot{U} = \frac{\partial}{\partial q_j}(H+U) M^{-1}_{ji} \frac{\partial}{\partial q_i}(H+U) = 0$). F. Cooper et al. [42] showed that any variational approximation to the dynamics of a quantum system based on Dirac action principle leads to a classical Hamiltonian dynamics for the variational parameters. Following Das [43], F. Cooper et al. introduced Poisson brackets by:

$$\{A, B\} = \frac{\partial A(q)}{\partial q_i} M^{-1}_{ij} \frac{\partial B(q)}{\partial q_j} .$$

They must obey Jacobi's identity:

$$\{q_i\{q_k, q_l\}\} + \{q_l\{q_i, q_k\}\} + \{q_k\{q_l, q_i\}\} = 0 ,$$

which is satisfied because $M_{i,j}$ obeys Bianchi's identity:

$$\frac{\partial M_{kl}}{\partial q_i} + \frac{\partial M_{ik}}{\partial q_l} + \frac{\partial M_{li}}{\partial q_k} = 0 .$$

Another interesting property is that eq.s. 3.4 are equivalent to the equation

$$\mathrm{Re}\left(\langle\, \delta\Psi_T \mid \left(i\frac{\partial}{\partial t} - H - 2U\right) \mid \Psi_T\rangle\right) = 0 , \tag{3.5}$$

where the variation $|\,\delta\Psi_T\,\rangle$ is done on the variational parameters, namely

$$|\,\delta\Psi_T\,\rangle = \delta q_i\, |\frac{\partial \Psi_T}{\partial q_i}\,\rangle . \tag{3.6}$$

3.3.2 Beyond the variational method

The Gross-Pitaevskii equation (GPE) can be numerically integrated, at least in simple geometries. We have developed a numerical scheme to solve GPE in one dimension and in tree dimensions with cylindrically symmetry. A fourth order Runge-Kutta method is used for the time integration.

We have found convenient to perform the numerical integration in real coordinate space (discretization of the spatial derivative) to reduce the computational effort. In fact, in such a way the GPE is reduced to a matrix form in which the self consistent field is diagonal (and then easily to numerically calculate) [2].

For each choice of the step length, we have a well defined "two well potential" tunneling problem which can be analyzed either by direct numerical integration or by the time dependent variational approach. Then the comparison between the two mode approximation has been done for each choice of the step length.

[2]The discretization in space breaks the global Galilean invariance and may introduces finite size spurious effect in the dynamics, if the velocity fields have a DeBroglie length of the order of the step length, which however can be easily controlled. Reducing the step length overcome the discretization problem. One could have used a set of basis functions to integrate the GPE. This would have the advantage to overcome the discretization problem, with a number of these functions less than the number of point in the grid, but the long CPU time needed to calculate the self consistent field could drastically reduce such advantages. (This would have overcome the discretization problem, but the number of these functions has to be finite in any numerical calculation, and this implies a cutoff in the kinetic energy.)

Chapter 4

The two mode approximation

4.1 Introduction

The time dependent variational two mode approximation (TMA) is a powerful tool to understand the low energy non linear dynamical behaviour of two weakly coupled Bose condensates. We consider a weak link between two Bose Einstein condensates, that can be realized in a two wells potential as described in the chapter 3. The external harmonic trap potential is assumed to be cylindrically symmetric (with a longitudinal frequency ω_0 and a radial frequency ω_r) and described by

$$V_{trap}\left(\mathbf{r}\right) = \frac{1}{2}m\omega_r^2\left(x^2+y^2\right) + \frac{1}{2}m\omega_0^2\, z^2 \ . \tag{4.1}$$

The double well potential is obtained by focusing an off-resonant laser sheet in the center of the trap (see also fig. 4.1). The laser barrier is assumed to be of gaussian shape

$$V_{laser}\left(z\right) = V_{laser}^0 \exp\left(-\frac{z^2}{l^2}\right) \ , \tag{4.2}$$

where V_{laser}^0 is proportional to the laser intensity. The dynamics of the "two" Bose Einstein condensates is described by the Gross-Pitaevskii equation (GPE)

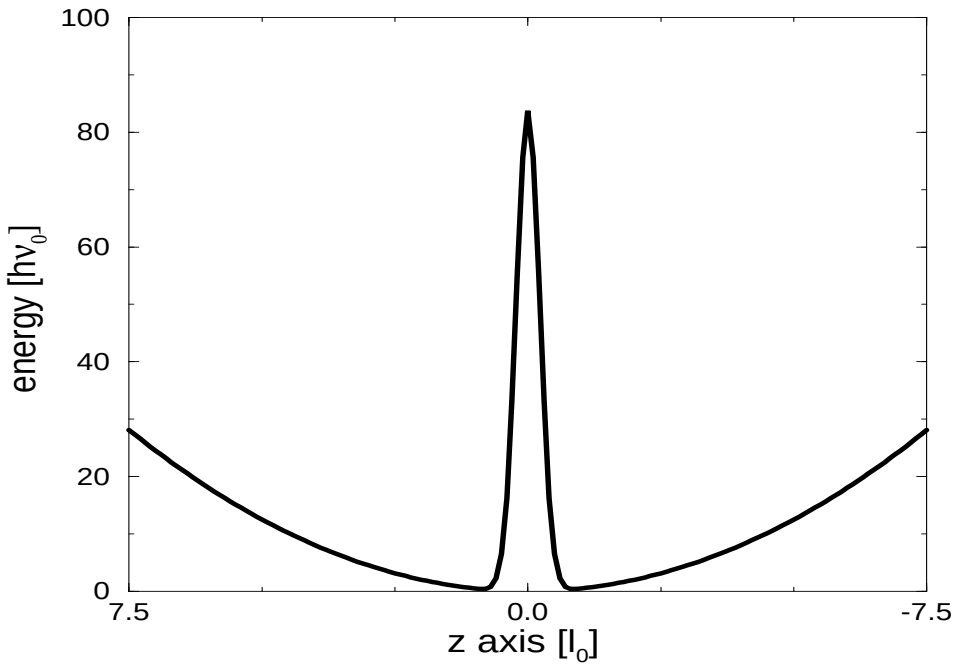

Figure 4.1: A double well potential can be created by focising a off-resonant laser sheet into the center of the magnetic (harmonic) trap.

2.1. We assume $V^0_{laser} > \mu$ where μ is the chemical potential at equilibrium (tunneling regime).

Now we suppose that Josephson-like tunneling through the barrier is the low energy dynamics of the GPE; in other words, the tunneling frequency is small as the lowest of the all possible intrawell frequency ($\sim \min(\omega_0, \omega_r)$); we will return later to this point when we will consider the full time-dependent integrations of the GPE in chapter 5.

In the next section we describe the time dependent variational two-mode approximation (TMA) applied to the two well potential system [17, 25]. Our approach is based on the time-dependent variational principle and we consider the Ansatz in which the trial macroscopic wave function is given by a superposition of two time-independent wave functions Ψ_1 and Ψ_2. Such functions Ψ_1 and Ψ_2 can be viewed as the lowest energy "stationary solution" of the left and right well respectively. In such a way a formal description in terms of the relative phase ϕ and the relative number δN can be obtained. These variables

are canonically conjugate and satisfy two coupled non linear eq.s. in terms of few static properties. It has to be noted that, although TMA is not expected to be a fully realistic approximation, nevertheless its formal scheme can be used as a guide of semiphenomenological treatments. We will show that, considering the various quantities appearing in the TMA equations as "effective" quantities, one can indeed obtain a very satisfactory description of the non linear tunneling dynamics.

In the third section we consider the problem of finding good trial wave function.

4.2 TMA: equations

In the time dependent variational two-mode approximation (TMA), the dynamics of the two coupled systems is constrained to a subspace spanned by two trial real wave functions Ψ_1 and Ψ_2.

$$\Psi = c_1\Psi_1 + c_2\Psi_2 \quad \text{where } \langle\Psi_1, \Psi_2\rangle = 0\,, \tag{4.3}$$

where the normalization are fixed by $\langle\Psi,\Psi\rangle = \langle\Psi_1,\Psi_1\rangle = \langle\Psi_2,\Psi_2\rangle = 1$. Therefore the amplitudes c_1, c_2 of the two wave functions are the unique dynamical amplitude to be determined. The physical meaning of $|c_1|^2$ is the fraction of atoms in the left well N_L/N . Symmetry arguments lead to the choice $\Psi_1(x,y,z) = \Psi_2(x,y,-z)$. The reduced Lagrangian of the TMA is

$$\begin{aligned} L &= \frac{1}{2}\hbar\left(ic_1^*\dot{c}_1 + ic_2^*\dot{c}_2 + h.c.\right) - E_0\left(c_1^*c_1 + c_2^*c_2\right) - h\left(c_1^*c_2 + c_2^*c_1\right) \\ &\quad -\frac{1}{2}U_0\left(|c_1|^4 + |c_2|^4\right) - \frac{1}{2}U_{12}\left(4|c_1|^2|c_2|^2 + \left(c_2^*c_1\right)^2 + \left(c_1^*c_2\right)^2\right) \\ &\quad -U_3\left(|c_1|^2c_1c_2^* + |c_1|^2c_1^*c_2 + |c_2|^2c_1c_2^* + |c_2|^2c_1^*c_2\right)\,, \end{aligned} \tag{4.4}$$

where E_0 and h are the diagonal and the out of diagonal matrix element of the single particle Hamiltonian (kinetic plus external potential energy), respectively:

$$E_0 = \int d\mathbf{r}\ \Psi_1(\mathbf{r})\left[-\frac{\hbar^2}{2m}\boldsymbol{\nabla}^2 + V_{ext}(\mathbf{r})\right]\Psi_1(\mathbf{r})\,, \tag{4.5}$$

$$h = \int d\mathbf{r}\ \Psi_1(\mathbf{r})\left[-\frac{\hbar^2}{2m}\boldsymbol{\nabla}^2 + V_{ext}(\mathbf{r})\right]\Psi_2(\mathbf{r})\,, \tag{4.6}$$

and

$$U_0 = g \int d\mathbf{r}\ \Psi_1(\mathbf{r})^4 \ , \tag{4.7}$$

$$U_{12} = g \int d\mathbf{r}\ \Psi_1(\mathbf{r})^2 \Psi_2(\mathbf{r})^2 \ , \tag{4.8}$$

$$U_3 = g \int d\mathbf{r}\ \Psi_1(\mathbf{r})^3 \Psi_2(\mathbf{r}) \, , \tag{4.9}$$

are the interaction terms. For repulsive interaction ($g > 0$) $U_0, U_{12} > 0$, whereas $(h + U_3) < 0$. The equations of motions follow from the standard Eulero Lagrange equation starting from the Lagrangian 4.4. The normalization $|c_1|^2 + |c_2|^2 = 1$ is a conserved quantity. Introducing the polar coordinate

$$c_i = \sqrt{n_i} \exp\left(-i\theta_i\right) \ , \tag{4.10}$$

one recovers that the fundamental variables of the problem are the phase difference $\theta = \theta_1 - \theta_2$ and the fractional[1] population imbalance $-1 < z = n_1 - n_2 < 1$. After some algebra one gets the following equations for z and θ

$$\hbar \dot{z} = 2\left(h + U_3\right)\sqrt{1 - z^2}\sin\left(\theta\right) + U_{12}\left(1 - z^2\right)\sin\left(2\theta\right) \ , \tag{4.11}$$

$$\hbar \dot{\theta} = -2\left(h + U_3\right)\frac{z}{\sqrt{1 - z^2}}\cos\left(\theta\right) + \left(U_0 \ - U_{12}\left(2 + \cos\left(2\theta\right)\right)\right) z \ . \tag{4.12}$$

The energy per particle is conserved by the dynamics described by the above eq.s.. We note that the z and θ variables are canonically conjugated, namely

$$\dot{\theta} = \frac{\partial}{\partial z}\left(\frac{H}{2}\right) \ , \tag{4.13}$$

$$\dot{z} = -\frac{\partial}{\partial \theta}\left(\frac{H}{2}\right) \ ,$$

where the Hamiltonian [2] is given by

$$H\left(z, \theta\right) = E_0 - E_J\sqrt{1 - z^2}\cos\left(\theta\right) + \frac{1}{4}U_0\ \left(1 + z^2\right) + \frac{1}{4}U_{12}\ \left(1 - z^2\right)\left(2 + \cos\left(2\theta\right)\right) \ . \tag{4.14}$$

In the above equation,

$$E_J \equiv -\left(h + U_3\right) \ , \tag{4.15}$$

[1] the wave function is normalized to one, then $n_1 \equiv N_1/N$ where N ,N_1 are the total number of atoms and the number of atoms in the left well respectively.

[2] If the term U_{12} can be neglected, H describes, in a simple mechanical analogy, a nonrigid pendulum, of tilt angle θ and a length proportional to $\sqrt{1 - z^2}$, that decreases with the "angular momentum" z .

is called the Josephson coupling energy (which is positive definite consistently with a ground state solution of the GPE without node) in closed analogy with Josephson coupling energy in Superconductor Josephson Junction. A physical interpretation of the Josephson coupling energy is also given in [19], where it is shown that it must depend only from the chemical potential and from the barrier potential.

4.2.1 The current-phase relation

It will be shown in the following that eq. 4.11 can be compared with the current-phase relation. If the solution of the GPE is a superposition of the two wave functions Ψ_1 and Ψ_2, as assumed in the Ansatz 4.3, the fractional atomic current flowing in the plane $z = 0$ is a *sinusoidal* current-phase relation

$$I = \frac{\hbar}{2m}\sqrt{1-z^2}\sin(\theta)\int_{-\infty}^{+\infty}dx\int_{-\infty}^{+\infty}dy\left(\Psi_1(\mathbf{r})\frac{\partial}{\partial z}\Psi_2(\mathbf{r}) - \Psi_2(\mathbf{r})\frac{\partial}{\partial z}\Psi_1(\mathbf{r})\right)_{z=0} . \tag{4.16}$$

This equation is obtained from the "microscopic" definition of current density and it is exact within the validity of the Ansatz 4.3. On the other hand, the fractional atomic current I must be also equal to the time derivative of the modulus square of the wave function integrated in the half space $z < 0$ (the local continuity equation is integrated in the half space)

$$I = \dot{n}_1 , \tag{4.17}$$

where

$$n_1 = \int_{-\infty}^{0}dz\int_{-\infty}^{+\infty}dx\int_{-\infty}^{+\infty}dy\ \left|\Psi(x,y,z)\right|^2 , \tag{4.18}$$

represents the fraction of atoms in the left well; n_1 is also related to the fractional population imbalance z by $n_1 = \frac{1}{2} + \left(\frac{1}{2} - R\right) z$ where $R = \int_{-\infty}^{0} dz\,|\Psi_2|^2$ is typically very small. Hence, using 4.17, the current I is related to the time derivative of the fractional population imbalance z by

$$I = \left(\frac{1}{2} - R\right)\dot{z} . \tag{4.19}$$

Inserting eq. 4.11 in the above equation one gets the result

$$I = (1-2R)\left(\frac{(h+U_3)}{\hbar}\sqrt{1-z^2}\sin(\theta) + \frac{U_{12}}{2\hbar}\left(1-z^2\right)\sin(2\theta)\right) . \tag{4.20}$$

The comparison between this equation and eq. 4.16 suggests that the TMA approximation can be applicable in the following case:

1. if $U_{12} \ll -(h + U_3)$,for each value of the phase difference θ and

$$I = (1 - 2R)\frac{(h + U_3)}{\hbar}\sqrt{1 - z^2}\sin(\theta) \ . \tag{4.21}$$

2. otherwise, if $U_{12} \sim -(h + U_3)$, this relation holds only for $\theta \ll 1$.

Therefore, since we are interested in the non linear dynamics, in which each value of the phase difference θ can occur, we assume that the term U_{12} is negligible.

Note also that eq. 4.21 differs from Cooper-pair SJJ tunneling current in its nonlinearity in z.

The detailed analysis of eq.s. 4.11 and 4.12 with exact analytical solutions in terms of Jacobian and Weierstrassian elliptic functions can be found in [18]. Here we describe only the main physical results (see also [17]).

4.2.2 Non-interacting limit case

For symmetric wells and negligible interatomic interactions ($U_0, U_3, U_{12} \ll h$), eq.s. 4.11 4.12 can be solved exactly, yielding Rabi-like oscillations with frequency

$$\omega_R = 2|h| \ . \tag{4.22}$$

Note that the eq.s. 4.11 and 4.12 in this case become

$$\begin{aligned} \hbar\,\dot{z} &= 2h\sqrt{1 - z^2}\sin(\theta) \ , \\ \hbar\,\dot{\theta} &= -2h\frac{z}{\sqrt{1 - z^2}}\cos(\theta) \ , \end{aligned} \tag{4.23}$$

and their solution is not trivial, unless one writes such equations in terms of the amplitudes c_1 , c_2.

4.2.3 Linear regime: Josephson plasma frequency

For symmetric wells the equilibrium value of the fractional population imbalance z_0 is equal to 0. Also the equilibrium value of the phase difference $\theta_0 = 0$.

The equations of motions 4.11 and 4.12 after linearization in $\delta z = z - z_0$ and $\delta\theta = \theta - \theta_0$ become

$$\begin{aligned} \hbar\,\delta\dot{z} &= -\left(-2h - 2U_3 - 2U_{12}\right)\,\delta\theta\,, \\ \hbar\,\delta\dot{\theta} &= \left(-2h - 2U_3 + U_0 - 3U_{12}\right)\,\delta z\,, \end{aligned} \tag{4.24}$$

and the dispersion relation[3] takes the form:

$$\hbar\,\omega = \sqrt{\left(-2h - 2U_3 - 2U_{12}\right)\left(-2h - 2U_3 + U_0 - 3U_{12}\right)}\,. \tag{4.25}$$

4.2.4 *The homogeneous limit case

The time dependent variational TMA, can be understood as an alternative way to perform an approximate description of the low energy dynamics and frequency. It can be applied not only to the double well potential (the case that it is considered in this chapter) but also to the study of each normal mode. Let me recall, that in the usual linearization of the GPE (as in the Bogoliubov approximation) the $U\left(1\right)$ symmetry is broken and the various observables[4] (except the energy) are not well defined to quadratic order in the displacements fields $\delta\Psi$ (see subsection 3 chapter 2 for the linearized GPE). In this sense it does not give a good description of the dynamics, although it gives the exact frequency of the small amplitude oscillations around the ground state (calculated with the GPE). In contrast TMA provides only an approximate value of this frequency, but the $U\left(1\right)$ symmetry is preserved and the various observables are well defined up to quadratic order in the displacement fields. In this sense it provides a good description of the dynamics.

It follows that, the TMA, with the appropriate choice of the trial wave function, can be used to describe low energy dynamics. It is worth mentioning an interesting work by Gardiner [37] in which a particle-number-conserving Bogoliubov method to describe low energy excitations is derived.

In the following, the linearized expression 4.25 is used for the calculation of the dispersion relations $\omega\left(k\right)$ in the homogeneous system; choosing $\Psi_1(\mathbf{r}) = 1/\sqrt{2} + \sin\left(\mathbf{kx}\right)$ and $\Psi_2(\mathbf{r}) = 1/\sqrt{2} - \sin\left(\mathbf{kx}\right)$ as variational wave functions, the integrals that appear in the Eq. 4.25 take the values $h = -\frac{\hbar^2 k^2}{4\,m}$, $U_0 = \frac{17}{8} g n_0$,

[3] This result has been obtained for an Hamiltonian that commutes with the axial symmetry $z \to -z$; the more general expression can be obtained by simple algebra.

[4] as for an example inteference between different mode.

$U_{12} = \frac{1}{8} g n_0$, $U_3 = -\frac{1}{8} g n_0$, where n_0 is the density. Using Eq. 4.25 the dispersion relation takes the form of the Bogoliubov result [33] for superfluid He^4

$$\hbar\,\omega\,(k) = \sqrt{\frac{\hbar^2\,k^2}{2m}\left(\frac{\hbar^2\,k^2}{2m} + 2gn_0\right)}\,, \tag{4.26}$$

which, in the long wavelength limit gives the linear dispersion $\omega\,(k) = \sqrt{\frac{gn_0}{m}}k$ (sound mode).

It is very important to note that the terms U_0, U_{12}, U_3, cannot be neglected. In particular, just neglecting the term U_{12} leads to a unphysical gap in the spectrum (see the previous discussion about the current phase relation in subsection $4.2.1$).

4.2.5 Non linear effects: self-trapped effect

A full solution of eq.s. 4.11 and 4.12 yields nonsinusoidal oscillations, that are the anharmonic generalization of the sinusoidal Josephson effect. Moreover, an additional novel nonlinear effect occurs in this model: a self-locked population imbalance [17]. Following the discussion about the current phase relation in subsection $4.2.1$, let us neglect the term U_{12} and rewrite eq.s. 4.11 and 4.12 using the time scale[5] $-2\,(h + U_3)\,/\,\hbar$:

$$\dot{z} = -\sqrt{1 - z^2}\sin\,(\theta)\,, \tag{4.27}$$

$$\dot{\theta} = \Lambda\,z + \frac{z}{\sqrt{1 - z^2}}\cos\,(\theta)\,, \tag{4.28}$$

where $\Lambda = -U_0/\,(2h + 2U_3) > 0$. We recall that the reduced energy

$$H = -\frac{1}{2}\sqrt{1 - z^2}\cos\,(\theta) + \frac{1}{4}\Lambda\,z^2 \tag{4.29}$$

is integral of motion. General solution of eq.s. 4.11 and 4.12 can be obtained by quadrature and can be found in [17][18]. Using the integral of motion to reduce the number of equations

$$\cos\,(\theta) = \frac{\frac{1}{2}\Lambda z^2 - 2H}{\sqrt{1 - z^2}}\,, \tag{4.30}$$

we get the following equation for $|\dot{z}|$

$$|\dot{z}| = \sqrt{1 - 4H^2 + (2\Lambda H\,-1)\,z^2 - \frac{1}{4}\Lambda^2 z^4}\,. \tag{4.31}$$

[5] this combination of energy integrals must be positive and corresponds to have a ground state solution without node.

Figure 4.2: Fractional population imbalance $z(t)$ versus rescaled time, with the initial conditions $z(0) = 0.6$, $\theta(0) = 0$, and $\Lambda = 1$ (a), and $\Lambda = 8$ (b), and $\Lambda = 9.99$ (c), and $\Lambda = 10$ (dashed line, d), and $\Lambda = 11$ (solid line, d).

From this equation follows that $z\,(t) = 0$ for some values of t if and only if $H \leq \frac{1}{2}$. Now looking this expression, it is evident that we have two types of solutions:

- 1) for $H < \frac{1}{2}$ solutions in z are symmetric and periodic around the equilibrium value $z_0 = 0$;
- 2) for $H > \frac{1}{2}$ solutions are not symmetric; i.e. the system dynamically breaks the symmetry; we refer to this non-linear effect as a self-locked population imbalance.

In the nonrigid pendulum analogy, this corresponds to an initial angular momentum $z\,(0)$ sufficiently large to swing the pendulum bob over the $\theta = \pi$ ver-

tical orientation, with a non zero $\langle z(t)\rangle$ time-average angular momentum corresponding to the rotatory motion.

The self-trapping of an initial BEC population imbalance is due to the atom-atom interactions in the Bose gas (non linear self-interaction in the GPE). It has a quantum nature, because it involves the coherence of a macroscopic number of atoms.

For $H = \frac{1}{2}$ we have a critical solution. We have also a critical fractional population difference z_c that represents also the maximal amplitude that can be supported by a generalized Josephson plasma oscillation (in the case $\Lambda > 1$)

$$z_c = 2\sqrt{\frac{1}{\Lambda} - \frac{1}{\Lambda^2}} \ . \tag{4.32}$$

For an initial condition $z(0) > z_c$, we have the self-locked population imbalance. For an initial condition $z(0) \gg z_c$ ($\Lambda \gg 1$), we have small oscillations of the differential population imbalance $z(t)$ around $z(0)$ with frequency $\Lambda z(0)$ and amplitude[6] $\frac{\sqrt{1-z(0)^2}}{\Lambda z(0)}$.

In the case $\Lambda \gg 1$ and $z \ll 1$ eq.s. 4.27 and 4.28 can be rewritten

$$\begin{aligned} \dot{z} &= -\sin(\theta) \ , \\ \dot{\theta} &= \Lambda z \, , \end{aligned} \tag{4.33}$$

and can take the equivalent form

$$\frac{1}{\omega_L^2}\ddot{\theta} = -\frac{d}{d\theta}V(\theta) \ , \tag{4.34}$$

where the "potential" is given by

$$V(\theta) \equiv 1 - \cos(\theta) \ . \tag{4.35}$$

Fig. 4.2 shows solutions of eq.s 4.27 and 4.28 with the particular initial conditions $z(0) = 0.6$, $\theta(0) = 0$, and with the parameter $\Lambda = 1, 8, 9.99, 10,$ and 11. The sinusoidal oscillations around $z = 0$ became anharmonic as Λ increases, fig. 4.2 (a), (b), and (c); in terms of energy these oscillations correspond to the value of $H = -0.31, 0.32, 0.4991$. The fractional population evolution $z(t)$ with the parameter $\Lambda = 10$ (fig. 4.2 (d, dashed line)) corresponds to the critical energy

[6] except around fixed point solution, in which the amplitude is not fixed, as we show in the following subsection.

value $H = 0.5$. For $\Lambda = 11$ (fig. 4.2 (d, solid line)) the population in each trap oscillates around a non-zero time average ($\langle z\,(t)\rangle \neq 0$); in terms of energy this corresponds to the value $H = 0.59$.

Figure 4.3: Constant energy lines in a phase-space plot of population imbalance z versus phase difference θ. Bold solid line: $z(0) = 0.6$, $\theta(0) = 0$, $\lambda = 1, 8, 10, 11, and 20$. Solid line: $z(0) = 0.6$, $\theta(0) = 0$, $\lambda = 0, 1, 1.2, 1.5,$ and 2.

The full dynamical behaviour of eq.s 4.27 and 4.28 is summarized in fig. 4.3, that shows the z-θ phase portrait with constant energy lines for different value of Λ, with initial conditions $\theta(0) = 0$ and $\theta(0) = \pi$, bold solid line and solid line, respectively. The bold solid line that cross the points $(\,z,\,\theta) = (\,0,\,(2n+1)\,\pi)$ corresponds to the critical energy value $H = \frac{1}{2}$.

4.2.6 Fixed points and π-state

Let us expand the reduced Hamiltonian around the stable fixed point. Around $z = z_0$ the energy is given by

$$\begin{aligned} H &\approx -\frac{1}{2}\sqrt{1-z_0^2}\cos(\theta) + \frac{1}{4}\Lambda z_0^2 \\ &+ \left(\frac{1}{2}\frac{z_0}{\sqrt{1-z_0^2}}\cos(\theta) + \frac{1}{2}\Lambda z_0\right)\delta z \\ &+ \frac{1}{4}\frac{1}{\left(\sqrt{1-z_0^2}\right)^3}\delta z^2\cos(\theta) + \frac{1}{4}\Lambda\,\delta z^2\,, \end{aligned} \tag{4.36}$$

where $\delta z = z - z_0$. The linear term in δz is equal to zero only if $\theta_0 = (2n+1)\,\pi$ and $z_0^2 = 1 - \frac{1}{\Lambda^2}$ (for $\Lambda > 1$). With this choice

$$H = \frac{1}{2}\left(\frac{1}{\Lambda} + \Lambda\right) + \frac{1}{4}\left(\Lambda^3 - \Lambda\right)\,\delta z^2 + \frac{1}{4}\frac{1}{\Lambda}\theta^2\,; \tag{4.37}$$

using $\dot{\theta} = 2\partial_z H = \left(\Lambda^3 - \Lambda\right)\,\delta z$ and $\delta\dot{z} = -2\partial_\theta H = -\frac{1}{\Lambda}\theta$ we obtain the frequency of the small oscillations

$$\omega_\pi^2 = \left(\Lambda^2 - 1\right)\,. \tag{4.38}$$

Solutions having π as a fixed point are denoted as π-states. In fig. 4.3 there is some example of solutions around π (solid line). The symmetrical solutions around the equilibrium position $z = 0$ correspond to $\Lambda < 1$, while self trapped solutions (around π) correspond to $\Lambda > 1$. The occurrence of similar solutions (also denoted π-states) have been recently observed in the Berkeley weak link experiments on superfluid ^{3}He-B [24].

The other fixed point with $z_0 = 0$ and $\theta_0 = 2n\,\pi$ and $\Lambda > 0$ corresponds to the usual Josephson plasma oscillation.

4.2.7 *TMA: non symmetric case

In the non symmetric case the equations of motions corresponding to eq.s. 4.11 and 4.12 become

$$\hbar\,\dot{z} = 2\,(h + U_{3m} + \Delta U_3\,z)\,\sqrt{1-z^2}\sin(\theta)\,, \tag{4.39}$$

$$\hbar\,\dot{\theta} = \Delta U + \Delta E - 2\,(h + U_{3m} + \Delta U_3\,z)\,\frac{z}{\sqrt{1-z^2}}\cos(\theta) + U_m\,z\,, \tag{4.40}$$

where

$$\Delta E = E_1 - E_2\,, \tag{4.41}$$

$$\Delta U = \frac{U_1 - U_2}{2}\,, \tag{4.42}$$

$$U_m = \frac{U_1 + U_2}{2}\,, \tag{4.43}$$

$$\Delta U_3 = \frac{U_{31} - U_{32}}{2}\,, \tag{4.44}$$

$$U_{3m} = \frac{U_{31} + U_{32}}{2}\ . \tag{4.45}$$

The terms E_1, E_2 and U_1, U_2 and U_{31}, U_{32} are obvious extensions of the integrals E_0, U_0, and U_3; where $U_1 = g \int d\mathbf{r}\ \Psi_1(\mathbf{r})^4$, and $U_{31} = g \int d\mathbf{r}\ \Psi_1(\mathbf{r})^3\Psi_2(\mathbf{r})$.

4.2.8 TMA versus an "effective" TMA

The analysis of the previous section has also a semiphenomenological character. The behaviour of the two coupled Bose gases is described in terms of a macroscopic phase difference θ and a fractional population difference z, whose equations of motion are given by eq.s 4.27 and 4.28, that depend parametrically on the ratio between the energy terms U_0 and $(h + U_3)$. We have discussed the dynamics without knowing the exact values of such energy terms. Such terms are geometry dependent: E_0 is a zero point energy of the single well, U_0 is proportional[7] to the mean field energy at equilibrium, and $(h + U_3)$ represents the critical current through the two wells. E_0, U_0 are bulk terms, whereas $(h + U_3)$ should depend only on the chemical potential μ and on the details of the barrier.

Hence the TMA can have a semiphenomenological meaning, and we will show that using proper "effective" values for U_0, $(h + U_3)$ one can get a reasonable agreement with the numerical solutions of the GPE.

4.3 TMA: variational functions and numeric implementation

In this section we discuss our procedure to find good trial functions $\Psi_1(\mathbf{r})$ and $\Psi_2(\mathbf{r})$ to get realistic estimate of the terms E_0, U_0, and $(h + U_3)$, for some geometries and for different parameters of the laser. In the previous sections we have

[7] four times in the double well symmetric potential.

performed a semiphenomenological analysis and now we go into a more microscopic one. We recall that the Ansatz 4.3 is that the trial wave function moves in a *two dimensional linear (complex) functional space*. We need some criteria to choose such reduced functional space in order to give a realistic estimate of the dynamics. Such reduced functional space is generated by two vectors, and it is natural to choose one of them as the ground state solution Ψ_0 of the Hartree equation [44]

$$\left(-\frac{\hbar^2}{2m}\boldsymbol{\nabla}^2 + V_{ext}\left(\mathbf{x}\right) + g\left|\Psi_0\right|^2\right)\Psi_0 = \mu_0\,\Psi_0\,, \tag{4.46}$$

and the other one as a vector Ψ_- that must have a node at $z = 0$. The usual left $\Psi_1\left(\mathbf{r}\right)$ and right $\Psi_2\left(\mathbf{r}\right)$ wave functions are given by

$$\Psi_1\left(\mathbf{r}\right) = \frac{1}{\sqrt{2}}\left(\Psi_0\left(\mathbf{r}\right) + \Psi_-\left(\mathbf{r}\right)\right)\,, \tag{4.47}$$

$$\Psi_2\left(\mathbf{r}\right) = \frac{1}{\sqrt{2}}\left(\Psi_0\left(\mathbf{r}\right) - \Psi_-\left(\mathbf{r}\right)\right)\,. \tag{4.48}$$

So, the question is what is the best choice of Ψ_- in order to better describe the lower energy tunneling dynamics. We have considered here only two particular choices for the variational wave function Ψ_-:

- the first odd *eigenstate Ψ_-^H of the Hartree Hamiltonian*[44]

$$\left(-\frac{\hbar^2}{2m}\boldsymbol{\nabla}^2 + V_{ext}\left(\mathbf{x}\right) + g\left|\Psi_0\right|^2\right)\Psi_-^H = \mu_-^H\,\Psi_-^H \tag{4.49}$$

- the first odd *self-consistent stationary solution Ψ_-^{SC} of the GPE*

$$\left(-\frac{\hbar^2}{2m}\boldsymbol{\nabla}^2 + V_{ext}\left(\mathbf{x}\right) + g\left|\Psi_-^{SC}\right|^2\right)\Psi_-^{SC} = \mu_-^{SC}\,\Psi_-^{SC}\,. \tag{4.50}$$

Ψ_-^H is consistent with the Bogoliubov dispersion relations for the homogeneous Bose system (see eq. 4.26). In fact the trials wave functions Ψ_1 and Ψ_2 used to obtain the results 4.26 are linear combinations of Hartree solutions (plane waves)

$$\Psi_1\left(\mathbf{r}\right) = \frac{1}{\sqrt{2}}\left(1 + \sqrt{2}\sin\left(\mathbf{k}\,\mathbf{r}\right)\right)\,, \tag{4.51}$$

$$\Psi_2\left(\mathbf{r}\right) = \frac{1}{\sqrt{2}}\left(1 - \sqrt{2}\sin\left(\mathbf{k}\,\mathbf{r}\right)\right)\,.$$

Using the Hartree wave function Ψ_{-}^{H} we have the relation:

$$-2\left(h+U_3\right)-2U_{12}=\mu_{-}^{H}-\mu_0=\frac{\hbar^2}{m}\frac{\int d\mathbf{r}\ \Psi_0\frac{\partial}{\partial x}\Psi_{-}^{H}}{\int d\mathbf{r}\ \Psi_0\, x\,\Psi_{-}^{H}}\,. \tag{4.52}$$

The rationale behind Ψ_{-}^{SC} is that, if ω_L is sufficiently lower than the bare harmonic frequency ω_0, the system is near the equilibrium and, if the phase difference is just π, Ψ_{-}^{SC} can be a good approximation for Ψ. Using the Self-Consistent wave function Ψ_{-}^{SC} we have the relation for the Josephson coupling energy (per particle)

$$E_J=-\left(h+U_3\right)=\frac{\epsilon_{-}^{SC}-\epsilon_0}{2}\,, \tag{4.53}$$

where ϵ_{-}^{SC} and ϵ_0 are the energy (per particle)[8] of the stationary solutions Ψ_{-}^{SC} and Ψ_0, respectively.

4.3.1 Numerical scheme for the stationary states of the GPE

The variational wave functions Ψ_0 , Ψ_{-}^{SC} and Ψ_{-}^{H} require only a static calculation. The first step is to find the total minimum Ψ_0 of the GP functional

$$H^{GP}=\int d\mathbf{r}\,\left(\Psi^* H_0\Psi+\frac{1}{2}g|\Psi|^4\right)\,, \tag{4.54}$$

where H_0 is the non interacting part of the Hamiltonian (kinetic plus external potential energy). Making use of the symmetry, we can work in the left well ($z<0$) only, imposing for Ψ_0 the boundary conditions $\frac{\partial\Psi_0}{\partial z}=0$ in the plane $z=0$ and with the normalization $\int|\Psi|^2=\frac{1}{2}$. The GP functional has been first discretized and then Ψ_0 has been obtained working in the real space as in the dynamical case discussed in section 3.3.2. We consider a dissipative (or damped) "dynamics" defined by the equation[9]

$$\dot{\Psi} \;=\; -\frac{\delta}{\delta\Psi^*}H^{GP}+\bar{\mu}\,\Psi\ , \tag{4.55}$$

$$\bar{\mu} \;\equiv\; \frac{1}{\int dr\ \ \Psi^*\Psi}\int dr\ \ \Psi^*\left(\frac{\delta}{\delta\Psi^*}H^{GP}\right). \tag{4.56}$$

These equations have two properties:

[8] namely $\epsilon=\mu-\frac{1}{2}\int d\mathbf{r}g\,|\Psi|^4$.

[9] Note that the dynamics we are referring to is not the dynamics of the Bose Condensate.

- 1) the energy reaches the minimum with a velocity proportional to the fluctuation in the chemical potential

$$\frac{d}{dt}H_{GP} = -2\int dr\ \Psi^*\left(H_0 + g|\Psi|^2\ \right)^2\ \Psi + 2\ \bar{\mu}^2\int dr\ \ \Psi^*\Psi \leq 0\,. \quad (4.57)$$

- 2) the normalization

$$\frac{d}{dt}\int dr\ \ \Psi^*\Psi = 0 \quad (4.58)$$

  is conserved.

The same technique is also used to find Ψ_{-}^{SC} with the boundary condition $\Psi_{-}^{SC} = 0$ in the plane $z = 0$. The dissipative dynamics 4.55 can also be adapted for the calculation of Ψ_{-}^{H}, starting from the Hartree energy functional

$$H^H = \int d\mathbf{r}\ \left(\Psi^* H_0\Psi + g|\Psi_0|^2|\Psi|^2\ \right)\ . \quad (4.59)$$

The "time" integration has been performed by using the fourth-order Runge-Kutta method. Working in the real space representation reduces the CPU time required for a single time iteration. The nonlinear interaction improves very much the efficiency of the algorithm (calculation of Ψ_0 and Ψ_{-}^{SC}).

Virial relations

We have used a spatial discretization scheme. As a convergency test, we have used the following virial relations (obtained by the scaling transformations $r_l \to \alpha\, r_l$):

$$U^{int} + T_r = V_r^{ho}\,, \quad (4.60)$$

$$\frac{1}{2}U^{int} + T_z + \langle\frac{z^2}{\lambda^2}V^{laser}\rangle = V_z^{ho}\,, \quad (4.61)$$

where U^{int} is the internal energy, T_z and T_r are the longitudinal and radial kinetic energy term respectively, V_z^{ho} and V_r^{ho} are the longitudinal and radial harmonic potential term respectively, V^{laser} the laser potential which is assumed of gaussian shape with a width $\sim \lambda$

$$U^{int} = \frac{1}{2}\,g\int dr\ \ |\Psi|^4\ , \quad (4.62)$$

$$T_x = \frac{\hbar^2}{2m}\int dr\ \ |\partial_x\Psi|^2\ , \quad (4.63)$$

$$V_x^{ho} = \frac{1}{2} m\,\omega_x^2 \int dr \;\; x^2\,|\Psi|^2 \;, \tag{4.64}$$

$$T_r = \frac{\hbar^2}{2m} \int dr \;\; \left(|\partial_y \Psi|^2 + |\partial_z \Psi|^2\right) \;, \tag{4.65}$$

$$V_r^{ho} = \frac{1}{2} m\,\omega_r^2 \int dr \;\; \left(y^2 + z^2\right) |\Psi|^2 \;, \tag{4.66}$$

$$V^{laser} \sim \int dr \;\; \exp\left(-\frac{x^2}{\lambda^2}\right) |\Psi|^2 \;, \tag{4.67}$$

$$\langle \frac{x^2}{\lambda^2} V^{laser} \rangle \sim \int dr \;\; \frac{x^2}{\lambda^2} \exp\left(-\frac{x^2}{\lambda^2}\right) |\Psi|^2 \;. \tag{4.68}$$

Note that virial relations 4.60 and 4.61 are valid for any self-consistent stationary solution of the GPE, therefore also for Ψ_{-}^{SC}.

Chapter 5

Numerical solution of the GPE

5.1 Introduction

In this chapter the predictions of the variational TMA are tested against a full numerical integration of the GPE for a double well geometry [25], which is related to the recent MIT experiments. We have done a few numerical studies for different values of the laser parameters. Here we limit to discuss the case of the laser parameters which provide a Josephson plasma frequency ω_L that does not satisfy the ideal condition $\omega_L \ll \omega_0$ for TMA, but rather $\omega_L \sim 0.15\ \omega_0$. Such a choice is due to the fact that in such regime one can expect deviations from the TMA and, on the other hand, this is a possible important range of ω_L from the experimental point of view. It is important to find the proper physical parameters of the laser barrier to reach a Josephson frequency ω_L of the same order of ω_0, so that a very low temperature is not needed for a clear experimental realization of the Josephson and self-trapped effects.

We have considered 10^4 Na atoms instead of the $5 \cdot 10^6$ of the MIT experiments. Calculations performed with $5 \cdot 10^3$ atoms have given results very close to the 10^4 case. One gets qualitative differences only below 10^2 atoms.

In section 2 the Josephson plasma frequency ω_L and the critical current E_J, calculated with the time dependent variational schemes, the one based to the Hartree Variational Basis (HVB) and the other one based to the Self Consistent Variational Basis (SCVB), are compared with the numerical results. The Josephson plasma frequency ω_L is calculated with the Bogoliubov approximation, and also by solving numerically the linearized GPE (by simple diagonalization scheme). The critical current is also determined studying directly the current-phase relation. The self trapping effect is also discussed.

The agreement between a TMA dynamics and the GPE is very good in the range of the coupling constant relative to the experimental situations and for Josephson frequency $\omega_L \leq 0.20\ \omega_0$ a sizeable decoupling from intrawell motions is observed.

5.2 Preliminary details

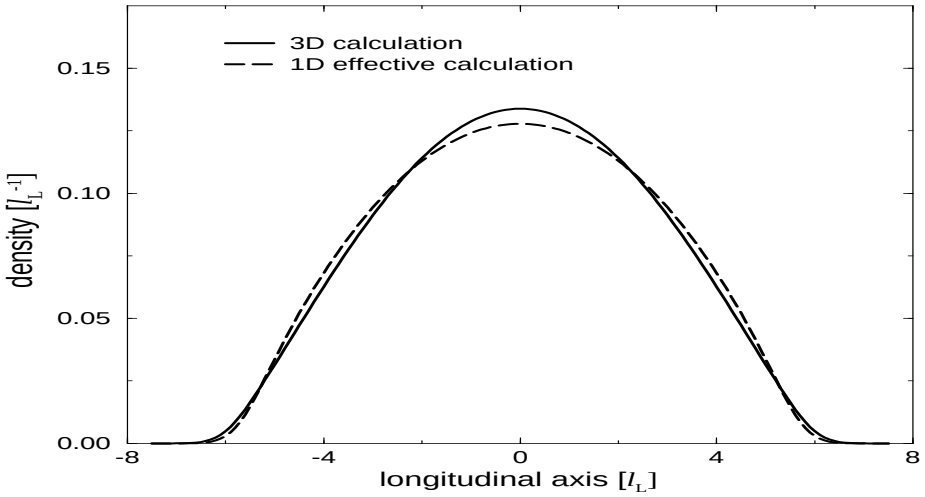

Figure 5.1: Equilibrium longitudinal density (integrated in the radial sections) for 10^4 Na atoms in the MIT trap with a longitudinal frequency $19\ Hz$ and a radial frequency $250\ Hz$. Energy and length scale are that of the longitudinal harmonic oscillator. The equilibrium density with a full $3D$ static calculation (solid line) is compared with the $1D$ effective calculation (dashed line). The detailed shape of the density is not important for the dynamics that we will study in this chapter.

We first analyzed to what extent the cigar shape geometry of the MIT experiment can be simulated by an "effective" $1D$ geometry. This is particularly

important because working with a $1D$ GPE (discretized) has the advantage that the Bogoliubov and Hartree diagonalization become accessible and a reasonable continuum limit can be achieved. With the $3D$ static calculation we found an effective radial section and from that an effective one-dimensional coupling g^{eff} has been estimated ($g^{eff} \sim 134$). Fig. 5.1 shows the longitudinal equilibrium density[1] for 10^4 atoms in the cigar-shaped trap of MIT ($3D$-calculation) and that obtained in the effective $1D$ geometry. One can see from this figure that the $1D$ effective geometry can be safely used to study the GPE dynamics. The $1D$ effective coupling g^{eff} calculated in the presence of the laser barrier differs the previous one only within $\sim 5\%$.

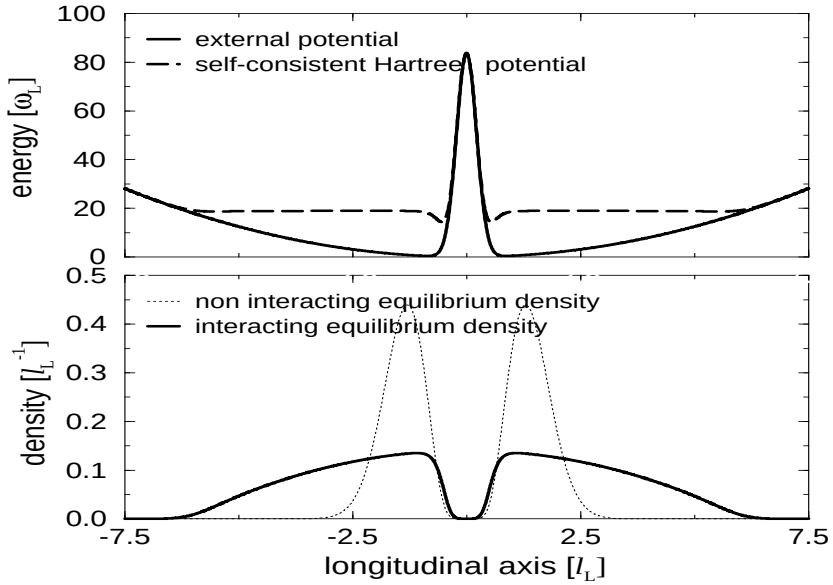

Figure 5.2: Potential profiles and equilibrium density in the longitudinal direction. A double-well potential can be created by focusing blue-detuned far-off-resonant laser light into the center of the magnetic trap (MIT protect[7]). The longitudinal $1/e^2$ half-width of the laser barrier is 0.3 μm and its heigth is 85 $\hbar\omega_0$. The top figure shows the external potential (solid line) and the self consistent Hartree potential (long dashed line), both calculated along the longitudinal line $x = 0, y = 0$. The bottom figure shows that the equilibrium density in the interacting case (considered) is strongly modified by the interaction. Despite the condensate seems well separated into two parts, the Josephson plasma frequency is ~ 0.15 $\hbar\omega_0$.

[1] the $3D$ density integrated on the radial sections.

Results for a particular choice of laser parameter (the longitudinal $1/e^2$ half-width of the laser barrier is $0.3\ \mu m$ and its height is $85\ \hbar\omega_0$) are discussed in the following.

The Josephson plasma frequency ω_L is approximately 0.15 of the bare frequency ω_0 (longitudinal frequency). Figure 5.2 (a) show the external potential (harmonic potential plus the laser potential which is assumed gaussian shaped) and the Hartree self-consistent potential. In figure 5.2 (b) the interacting equilibrium density is compared with the non interacting one. It is interesting to note that, despite the fact that the interacting tunneling frequency is not too small compared with the bare ω_0, the condensate appears well separated into two parts.

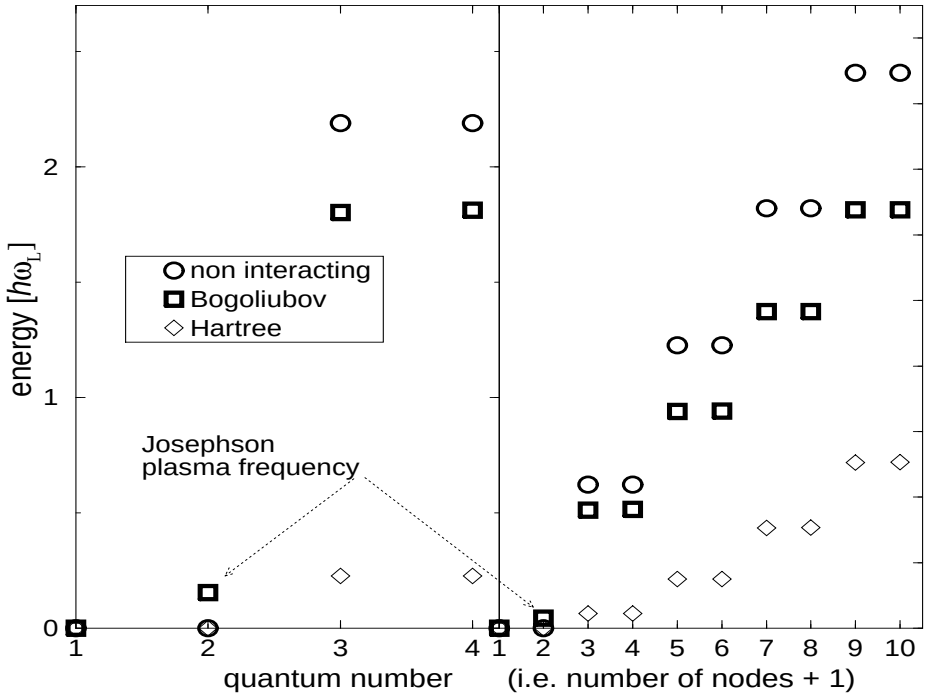

Figure 5.3: Energy level: interacting (squares) versus non interacting (circles). The left figure is a zoom of that on the right. Hartree energies (diamonds), are showed only for reference, and must not be confused with that ones calculated with TMA. Energy levels are ordered as a function of the number of nodes and referred to the ground state (labeled by 1). Energy levels are naturally grouped in couples of quasi degenerate energy levels; the small shift (almost not visible) is due to the weak coupling of the "two" condensates. It is interesting to note that only in the first excited level (labeled by 2), that correspond to ω_L, is strongly modified by the interaction.

The Bogoliubov energy spectrum is given in fig 5.3 together with the corresponding spectrum in the non interacting case. The figure on the left is a zoom of the figure on the right. Circles are relative to the non interacting case and square are relative to the Bogoliubov linearization. Diamonds are the energy of the Hartree states, that we show only for reference (energy eigenvalues must not be confused with the TMA frequency calculated with the Hartree states). Energy levels are ordered as a function of the number of nodes and referred to the ground state (labeled by 1). Energy levels are grouped in couples of quasi degenerate energy levels; the small shift (almost not visible) is due to the weak coupling of the "two" condensates. It is interesting to note that only in the first excited level (labeled by 2), the Josephson plasma frequency ω_L, is strongly modified by the interaction. Its value differs by several (~ 8) orders of magnitude with respect to that of the non interacting tunneling case.

5.3 Linearized dynamics and Current-Phase relation

The numerical values of the energy integrals (h, U_0, U_3, U_{12} defined in eq.s. 4.6, 4.7, 4.8, and 4.9, respectively) that appear in the TMA, evaluated with the Hartree variational basis (HVB) and the Self-Consistent variational basis (SCVB) are compared below

	HVB	SCVB
U_0	28.0	28.1
U_3	138.3 e-4	6.0 e-4
$-(h+U_3)$	8.8 e-4	5.2 e-4
U_{12}	3.7 e-4	8.5 e-7

The term U_0 is a bulk term and depends very weakly from the choice of the trial wave function. In the equations of motion the terms h and U_3, appear in the combination $h+U_3$; it is worth notice that the mean field term U_3 cannot be neglected in the geometries that we have considered. In the HVB the term U_{12} is not negligible compared to $h+U_3$, while in the SCVB the term U_{12} is negligible.

The calculation of the Josephson plasma frequency with HVB, SCVB and linearized GPE (Bogoliubov approximation) gives the following results

	HVB	SCVB	Bogoliubov
ω_L	0.169	0.170	0.15

Both variational basis, HVB and SCVB, provide similar results for the Josephson plasma frequency, despite the fact that the values of the term U_{12} are very different. Both are an upper bound of the exact Bogoliubov result. Fig. 5.4

Figure 5.4: Josephson frequency, calculated with Bogoliubov (1), HFVB (2), SCVB(3), versus different values of the laser power (arbitrary units). In wide range HFVB, SCVB agree and approximate the Bogoliubov dispersion a part from a constant shift.

shows the Josephson plasma frequency ω_L in a wide range of the laser power. Josephson plasma frequencies are calculated both with Bogoliubov, with the SCVB , and with HVB. The calculated ω_L with SCVB and HVB agree well each other and differ from the exact linearization by a $\sim 10\%$ quite independently from the barrier height (laser power).

Finally fig. 5.5 shows the current-phase relation obtained by integrating numerically the time-dependent GPE. It is almost a sinusoidal function and agrees very well with the TMA current phase relation given by the SCVB. HVB results for the current phase relation agree with the numerical results only for very small phase difference ($\theta \leq 0.01$).

It is important to notice that the main reason why SCVB provides a better description of current phase relation is because U_{12} is much smaller than in HVB. This feature is quite general. TMA fails in the description of the non linear dynamics when the U_{12} energy integral is comparable with the combination $-(h + U_3)$ (see the discussion on the current phase relation in subsection $4.2.1$).

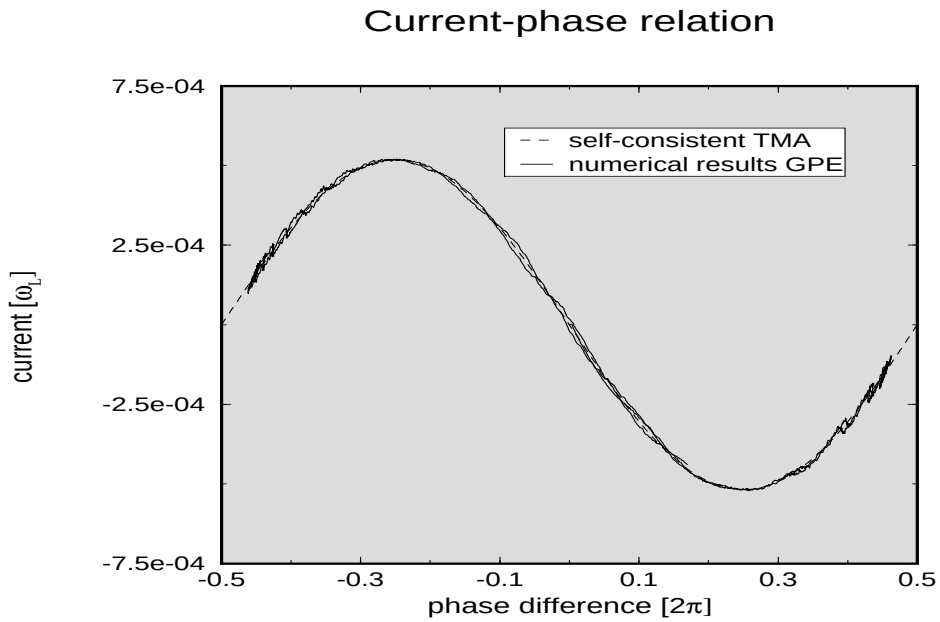

Figure 5.5: Solid line correspond to the numerical integration of the GPE; longh-dashed line correspond to the sinusoidal current-phase obtained in the TMA.

The small deviations of TMA with respect to the numerical results appearing in fig. 5.5 are not due to numerical errors, but to the coupling with the intrawell motions. Such deviations totally disappear in the limit of small Josephson plasma frequency.

5.4 Non linear Josephson-like oscillations

One of the most relevant prediction of the variational TMA is the occurring of the so called Self-Trapped effect [17], when the initial imbalance is larger than a critical value z_c (see eq. 4.32). This is confirmed by the numerical solution of the GPE under the condition $\omega_L \leq 0.20\ \omega_0$ and $U_0\, z \leq \hbar\omega_0$. Fig. 5.6 shows the evolution of the fractional population imbalance $z(t)$ for some initial values $z\,(0)$ chosen around its critical value z_c. For $z \geq z_c$ Self-Trapping occurs, i.e. the population in one well oscillates around a value that is not the equilibrium value $z = 0$; in figure 5.6 the solution with initial conditions $z\,(0) \approx 0.015$ and $\theta\,(0) = 0$ is a self trapped one; it oscillates around $z \approx 0.010$, without passing through the zero. The critical solution, corresponding to the initial condition $z\,(0) = z_c \approx 0.013$ and $\theta\,(0) = 0$, is not a periodical solution. For $z \approx z_c$ anharmonical

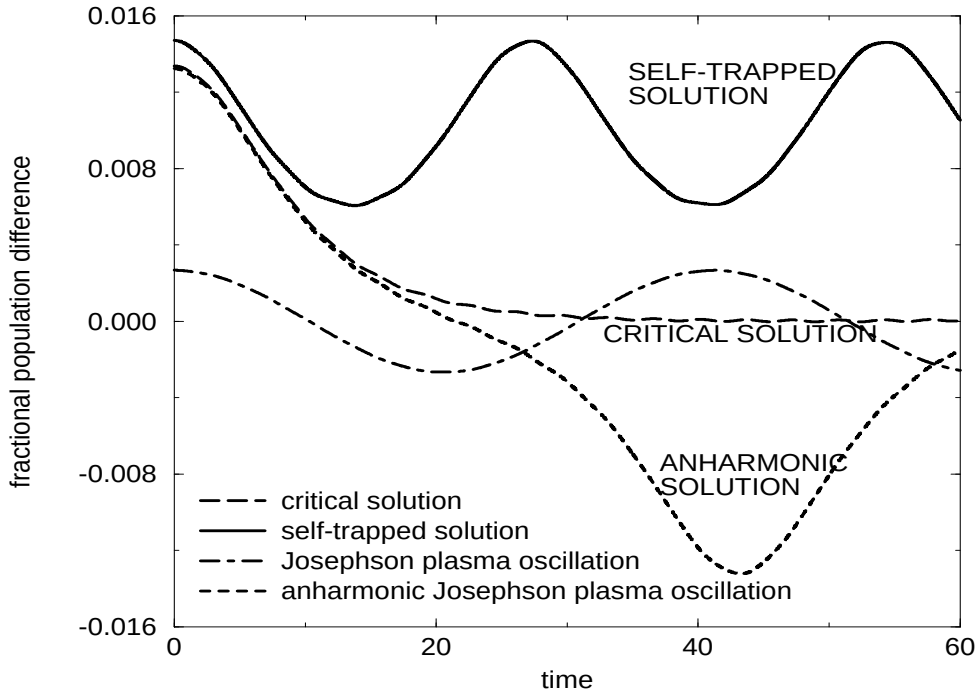

Figure 5.6: Numerical GPE results for the fractional population imbalance evolutions $z(t)$ for different values of the initial condition $z(0)$ near the critical value z_c, and with $\theta(0) = 0$.

oscillations occur while for $z \ll z_c$ one has harmonical oscillations. Self trapped solutions for $z \gg z_c$ are harmonical.

5.5 Effective TMA

The numerical integrations of the Gross-Pitaevskii equation (GPE) in a one-dimensional double well potential shows a qualitative agreement with the self consistent variational TMA. In particular excellent agreement is obtained for the critical current (with typical relative precision 0.1%) and the current-phase relation. However, in general one cannot expect an excellent quantitative description of the non linear tunneling dynamics, because the variational two mode ansatz is only an approximate one. However the variational TMA can be very useful to give a semiphenomenological set of equations of motion for the relevant quantities. Let us rewrite the TMA equations (see eq. 6.20 and 6.21) in the

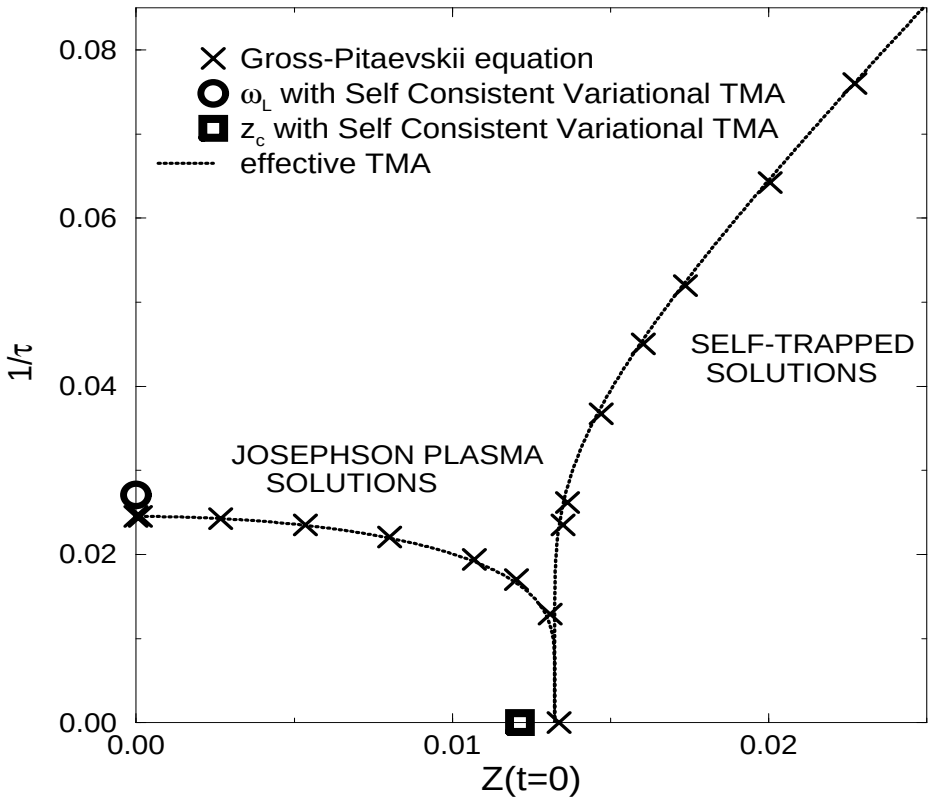

Figure 5.7: Frequency of the nonlinear Josephson oscillations versus different values of z in the range of its critical value z_c; the initial phase difference is zero.

form

$$\hbar\,\dot{z} = -2E_J^*\sqrt{1-z^2}\sin(\theta)\,, \tag{5.1}$$

$$\hbar\,\dot{\theta} = 2E_J^*\frac{z}{\sqrt{1-z^2}}\cos(\theta) + U_0^*\,z\,, \tag{5.2}$$

where the relevant physical quantities U_0^*, E_J^* are "phenomenological" inputs. In this case these "phenomenological" inputs are obtained from the numerical solutions of the GPE:

- Josephson energy coupling is obtained analyzing the current phase relation

$$E_J^* = \hbar I_c \approx 5.2\cdot 10^{-4} \qquad E_J^{SCVB} \approx 5.2\cdot 10^{-4}$$

(where the critical current I_c is the maximal value of the current I_c)

- the mean field term U_0^* should be obtained by the frequency ω_L of the low energy Josephson plasma oscillation

$$U_0^* \equiv \frac{\hbar\omega_L^2}{2I_c} \approx 21.9 \qquad U_0^{SCVB} \approx 28.1$$

These values lead to excellent results. The critical value of the population imbalance z_c is reproduced within 1%. Both shape and frequency of the non sinusoidal Josephson oscillations are reproduced with the same accuracy. Fig. 5.7 summarizes these results: the period of oscillation is displayed as a function of the initial value $z\,(0)$ in a range of values around its critical value of z_c (and with $\theta\,(0) = 0$).

5.6 Discussion

The numerical integration of the Gross-Pitaevskii equation (GPE) in a double well potential proves that the low energy tunneling dynamics is accurately described by an effective two mode approximation. The non-linear dynamical behaviour of the two weakly coupled BECs can be described in terms of a macroscopic quantum phase-difference and in terms of the population difference between the two sub-systems. The macroscopic quantum phase-difference and the population difference satisfy a nonlinear equation in which only two energy scale are present, the Josephson coupling energy E_J and a bulk energy E_C. In particular one of these can be used as unit scale reference and the coefficients in the equations depend only on the ratio between the two energy integrals. The values of the Josephson coupling energy and the bulk energy can be extracted studying the current phase relations and the frequency of the low-living excitations (the Josephson plasma frequency) of the GPE. Using these "phenomenological" values it is possible to reproduce a large variety of effects typically of the TMA.

In the last section 5.5, we have observed that, despite the self consistent variational TMA give a systematic error in the calculation of Josephson frequency the non-linear dynamics is well described. We have proved that the TMA equations, after the substituting I_c and ω_L calculated on a variational basis, with those determined by the mean field dynamics, reproduce with an excellent approxi-

mation the non linear low energy dynamics. This feature is quite general and the accuracy increases as ω_L/ω_0 decrease.

The bulk energy in the variational TMA is essentially independent from the choice of the variational function and it is typically an upperbound ($10 \div 20$ %) with respect to the "phenomenological" value obtained studying numerically the GPE. Such energy shift between variational bulk energy and the phenomenological value is a clear signature that the exact low energy mean-field dynamics of the wave function is not well described by an evolution in a two dimensional (complex) functional space.

Chapter 6

An analog of the Josephson effect (dc $I - V$ curve)

6.1 Introduction

One of the proposed way to obtain a BEC weak-link, extensively discussed in the previous chapters, is based on a double-well potential created by focusing an off-resonant laser light into the center of the magnetic trap [17].

Theoretical calculations show that (in a typical experimental setup), despite the fact that the frequency scale of Josephson plasma oscillation ω_L can be a fraction not necessarily small of the typical trapping frequencies, the maximal amplitude of Josephson population oscillations could be low for the present resolution of the available experimental setups. Therefore the direct observation of Josephson oscillations as well as the measure of both the plasma frequency ω_L and the critical current I_c could be difficult.

In this chapter we suggest a strategy to improve the observability of the non-linear effects of the interaction [26]. We propose an experiment based on the possibility of a slow relative motion of the trapping potential with respect to

the laser sheet. We will show that if the relative velocity v_r is sufficiently slow ($\sim 0.1\ \mu m/s$), no chemical potential difference between the two wells occurs and a finite superfluid current[1] flows through the tunneling barrier to maintain the chemical potential equilibrium. Then we will see that a critical value of the relative velocity v_r^c exists for the occurrence of the critical effects of the interaction (Self Trapping). Under the critical value v_r^c a macroscopic and observable flux of atoms can be produced. We will show that this strategy leads to an indirect measure of the critical current I_c and the Josephson plasma frequency ω_L, even in the case in which the Josephson oscillations cannot be directly observed.

We suggest to experimentally investigate a phenomenon that is the close analog of that occurring in a single Superconductor Josephson Junction (SJJ) under the action of an external dc current source[2] [45]. The role of the external electric circuits with a current source is played by the relative motion of the laser and the magnetic trap and *the analog of the dc and ac effects* can be formally recovered. The relative velocity v_r corresponds to the intensity of the external applied current in SJJ. The *dc $I - V$ curve*, $V = V(I)$ can be explored.

To theoretically investigate this "experiment" we have used methods similar to those described in the previous two chapters. We will first discuss some analytical approximations based on the TMA. Then we will substantiate these approximations showing that results from a numerical integration of the GPE agree with those from the effective TMA (in chapter 7).

The chapter is organized as follows. The underlying physical idea is given in section 2. A semiphenomenological treatment based on an effective time-dependent TMA is discussed in sections 3 and 4, together with the explanation of the origin of the critical value for the relative velocity v_r^c. A relation between the effective parameters is also discussed in section 4. The last section is devoted to a summary.

[1] The superfluid current component is approximatively constant (DC component).
[2] (or also under the action of a slowly varying current).

6.2 A moving laser improves the observability

Let us consider the harmonic trapping potential with cylindrical symmetry (with a longitudinal frequency ω_0 and with a radial frequency ω_r) given by

$$V_{trap}(\mathbf{r}) = \frac{1}{2}m\omega_r^2\left(x^2+y^2\right) + \frac{1}{2}m\omega_0^2\, z^2\,. \tag{6.1}$$

At $t \leq 0$ a barrier potential, that can be created by focusing an off-resonant laser sheet into the center of the trap, is described by the gaussian shaped potential given by

$$V_{laser}(z) = V_{laser}^0 \exp\left(-\frac{z^2}{l^2}\right)\,. \tag{6.2}$$

The laser starts moving at $t = 0$ in the longitudinal direction (the z axis) with constant velocity v_r. It is possible to show (also by the numerical integration of GPE), that if it is the trap to move instead of the laser, we obtain the same dynamics[3], that we will discuss. The time dependent external potential is then given by the sum of the trapping potential $V_{trap}(\mathbf{r})$ and the laser barrier potential $V_{laser}(z - v_r t)$

$$V_{ext}(\mathbf{r},t) = V_{trap}(\mathbf{r}) + V_{laser}(z - v_r t)\ , \tag{6.3}$$

where

$$\text{for } t < 0 \quad \text{we assume} \quad v_r = 0\,. \tag{6.4}$$

We will consider values of v_r much smaller than the maximal sound velocity. The populations N_1 and N_2 of the left and right well, respectively, are defined by

$$N_1(t) \equiv N\int_{-\infty}^{v_r t} dz \int\int dxdy\,|\Psi(\mathbf{r},t)|^2\,, \tag{6.5}$$

$$N_2(t) \equiv N\int_{v_r t}^{\infty} dz \int\int dxdy\,|\Psi(\mathbf{r},t)|^2\,, \tag{6.6}$$

(where $v_r t$ is the longitudinal position of the laser sheet). Let us assume that the system is in the equilibrium configuration for $t < 0$ and then the initial conditions are

$$N_1(0) = N_2(0) = N/2. \tag{6.7}$$

[3]Moving the trap instead of the laser, due to Galilean invariance, leads to the same equations for the relevant macroscopic observables. Only the initial condition can change, but for the values of velocities considered such modifications are negligible.

We will show with the direct numerical integration of the GPE (chapter 7) that if the velocity v_r is smaller than a critical value v_r^c the population imbalance $\Delta N(t) \equiv N_1(t) - N_2(t)$ can be estimated by approximating the condensate wave function $\Psi(\mathbf{r},t)$ by a quasi-stationary solution $\Psi_0(\mathbf{r},t)$ of the GPE given by

$$\mu_0(t)\,\Psi_0(\mathbf{r},t) = -\frac{\hbar^2}{2m}\boldsymbol{\nabla}^2\Psi_0(\mathbf{r},t) + \left[V_{ext}(\mathbf{r},t) + g\,|\Psi_0(\mathbf{r},t)|^2\right]\Psi_0(\mathbf{r},t)\ . \quad (6.8)$$

where $\mu_0(t)$ is weakly time dependent[4]. We also assume that $V_{ext}(\mathbf{r},t) > \mu_0(t)$, i.e. that we are in the tunneling regime. For the laser displacements $a = v_r t$, that we will consider, ΔN is approximately proportional to a. Since the experimental accuracy in measuring the condensate density with non destructive techniques is about 10%, the laser displacement must be sufficiently large to have a value for ΔN which is measurable.

As usual, we assume that the lifetime of the condensate is long compared to the scale of Josephson oscillations. From the experimental point of view, the lifetime of the condensate can be a practical limitation. For this reason it is better to analyze the dependence of the population on the velocity v_r, fixing the time interval t_f of the laser motion rather then its total displacement. Then ΔN is observed after the time t_f, and it is a function $\Delta N(v_r)$ of the velocity v_r.

We will also demonstrate that, above the critical velocity v_r^c, the approximation 6.8 breaks abruptly and the flux $\Delta N(v_r) \sim 0$. The actual experimental observation of this sudden change in ΔN gives a measure of v_r^c. The strategy described here improves the observability of the Josephson-like effects since, although "plasma" oscillations can be difficult to observe, both the critical current I_c and the Josephson plasma frequency ω_L can be indirectly determined from the experimental values of v_r^c and $\Delta N(v_r \simeq v_r^c)$.

In fact, we will show that I_c and ω_L can be obtained by the following eq.s[5]

$$I_c \simeq \frac{\Delta N(v_r^c)}{t_f}\,, \quad (6.9)$$

[4] Although this approximate solution $\Psi_0(\mathbf{r},t)$ is a real function and therefore current density cannot be calculated directly from it, the time dependence of the population imbalance between the two wells $\Delta N(t)$, can be realistically calculated.

[5] We have omitted for simplicity a common factor in both the equations. This factor $(1/0.72)$ depends on the initial condition 6.4 and it will discussed in section 6.3.3. In the case in which the laser acquires its velocity very slowly (in the time scale $1/\omega_L$) this factor must be omitted. It is possible to show that also in presence of strong damping this factor must be omitted.

$$\omega_L^2 \simeq \frac{2F}{\hbar}\, v_r^c\,, \tag{6.10}$$

where the average force F is given by[6]

$$F = -m\,\omega_0^2 \int d\mathbf{r}\; z\;|\Psi_1|^2\;. \tag{6.11}$$

6.2.1 How can the population difference be measured?

Recently a new technique of observing dynamical processes it was used to study the propagation of sound in elongated cloud of Bose-Einstein condensates [9]. Impressive pictures of moving condensates have been taken using phase-contrast imaging. This method seems to be within a good approximation a quantum nondemolition measurement[7] (for a recent discussion see [**?**][46]). Non-resonant laser light illuminates the sample, travels through, and attains phase shifts that are proportional to the density of the condensate. The acquired phase gradient is measured using the non-scattered part of the incident light as a reference.

This method seems an excellent candidate for monitoring the population difference in the two well potential. In particular this technique developed for rapid sequence of imaging of sound propagation can be adapted and improved for the case in which the time scale of the dynamics is much longer than that of the sound propagation. For our proposed experiment is necessary and sufficient the knowledge only of the initial and final population difference (also initial because is too difficult to cut the condensate exactly in the middle, see the pictures in [9]).

6.3 A simple theoretical model

The simplest but still realistic model to study the proposed physical system is based on the variational TMA, in which the low energy solution of the GPE is written as a superposition of two static wave functions $\Psi_{1,2}(\mathbf{r})$ with complex time dependent amplitude $\sqrt{n_{1,2}(t)}\exp(-i\theta_{1,2}(t))$. In the previous chapter we

[6] F is the average force, that the condensate atom in the left well fills, induced by the moving laser barrier and $F v_r^c\, t$ represents the corresponding average work. The condensate atoms, "localized" in the left well, are in a quasi stationary state; then the force that the laser barrier played on these atoms is equal and opposite to the force played by the harmonical trap.

[7] which means that the measurement does not modify significantly the condensate.

have shown that a good choice for the variational wave functions $\Psi_i(\mathbf{r})$ is given by the combination even and odd of the low energy self-consistent stationary solutions[8] $\Psi_\pm$ of the time-independent GPE

$$\left(-\frac{\hbar^2}{2m}\boldsymbol{\nabla}^2 + V_{ext}\left(\mathbf{r},0\right) + g\left|\Psi_\pm\right|^2\right)\Psi_\pm = \mu_\pm\,\Psi_\pm\,, \tag{6.12}$$

where $\int d\mathbf{r}\left|\Psi_\pm\right|^2 = 1$ and $\Psi_+ = \Psi_0$ (the ground state solution of the GPE). The dynamical behaviour of the fractional population imbalance $z = n_1 - n_2$ and the phase difference $\theta = \theta_1 - \theta_2$ depends only through few energy integrals: the Josephson coupling energy E_J, the capacitive energy E_c, and the "zero point" energy difference $\Delta E\left(t\right)$. We calculate such terms when the laser is positioned in the middle of the trap (we take advantage from the symmetry setting $\Psi_1\left(x,y,z\right) = \Psi_2\left(x,y,-z\right)$). We have shown in the previous chapters that E_J is related to $\Psi_\pm$ by $2E_J = \epsilon_+ - \epsilon_-$ where $\epsilon_\pm$ are the respective values of the energy per particle[9] and E_c arises from the mean field $E_c = U_0 = g\int d\mathbf{r}\ \Psi_1(\mathbf{r})^4$. Let us consider the case in which E_J is several orders of magnitude lower than U_0, typically $4 \div 6$ order of magnitude. Then the maximal amplitude of the Josephson plasma oscillation (which coincides with the critical value (eq. 4.32) $z_c = 2\sqrt{2E_j/U_0 - \left(2E_j/U_0\right)^2}$) is of order $.02 \div .002$.

The moving laser induces a time-dependent energy (per particle) difference

$$\Delta E\left(t\right) = E_1 - E_2\,, \tag{6.13}$$

in the two well, where

$$E_{1(2)} = \int dr\ \Psi_{1(2)}\left[-\frac{\hbar^2}{2m}\nabla^2 + V_{ext}\left(\mathbf{r},t\right)\right]\Psi_{1(2)}\ . \tag{6.14}$$

If we linearize $\Delta E\left(t\right)$ in the time t around $t = 0$ (i.e. when the laser is in the middle of the trap), we get

$$\Delta E\left(t\right) = 2F\,v_r t\,, \tag{6.15}$$

where v_r is the relative drift velocity and where F is given by

$$F \equiv \int dr\ \frac{\partial V_{laser}\left(r\right)}{\partial x}\left|\Psi_1\right|^2 = u_l\left(-2\int dr\,\frac{x}{\lambda^2}\exp\left(-\frac{x^2}{\lambda^2}\right)\left|\Psi_1\right|^2\right)\ . \tag{6.16}$$

[8] i.e. $\Psi_1 = \left[\Psi_+ + \Psi_-\right]/\sqrt{2}$ and $\Psi_2 = \left[\Psi_+ - \Psi_-\right]/\sqrt{2}$.

[9] namely $\epsilon_\pm = \mu_\pm - \frac{1}{2}\int d\mathbf{r} g\left|\Psi_\pm\right|^4$.

and represents the average force per atom in the single left (1) well induced by the laser barrier. Note that for symmetry reasons this force is equal and opposite to that one calculated in the right well (2)

$$F \equiv \int d\mathbf{r} \ \frac{\partial V_{laser}\left(\mathbf{r}\right)}{\partial z} \left|\Psi_1\right|^2 = -\int d\mathbf{r} \ \frac{\partial V_{laser}\left(\mathbf{r}\right)}{\partial z} \left|\Psi_2\right|^2 \quad . \tag{6.17}$$

But the same force integral F can be also calculated using the fact that Ψ_1 is quasi-stationary in the sense that Ψ_1 must satisfy within a good approximation the stationary equation

$$\int d\mathbf{r} \ \frac{\partial V_{ext}\left(\mathbf{r}\right)}{\partial z} \left|\Psi_1\right|^2 \simeq 0 \quad . \tag{6.18}$$

Then the force integral F can be also calculated by using the following expression

$$F \simeq -m\,\omega_0^2 \int d\mathbf{r}\, z \ \left|\Psi_1\right|^2 \tag{6.19}$$

If one approximates the expression 6.16 with 6.19, the relative error introduced is typically less then 0.1%. An important point is that the integral 6.19 does not depend very much from the details of the laser potential. It can be also evaluated with the static Thomas-Fermi approximation with only few $\%$ of relative error.

6.3.1 The analog of the DC Josephson equations

Within the TMA we obtain the following equations of motion for the relative population $z = n_1 - n_2$ and the relative phase $\theta = \theta_1 - \theta_2$

$$\hbar\,\dot{z} \ = \ -2E_J\sqrt{1-z^2}\sin\left(\theta\right) \ , \tag{6.20}$$

$$\hbar\,\dot{\theta} \ = \ \Delta E\left(t\right) + 2E_J\frac{z}{\sqrt{1-z^2}}\cos\left(\theta\right) + U_0 \ z \, , \tag{6.21}$$

where

$$\Delta E\left(t\right) = 2F\,v_r t \ , \tag{6.22}$$

Let us consider the case $E_J \ll U_0$, namely let us neglect the second term in the right hand side of Eq. 6.21. To simplify the discussion, we consider $z \ll 1$, $\sqrt{1-z^2} \sim 1$. From eq.s. 6.20 and 6.21 one gets the result

$$\frac{1}{\omega_L^2}\ddot{\theta} = -\frac{d}{d\theta}V\left(\theta\right) \ , \tag{6.23}$$

where the effective potential $V(\theta)$ is given by

$$V(\theta) \equiv \tilde{I}\,\theta + 1 - \cos(\theta)\ , \tag{6.24}$$

with $\tilde{I} \equiv 2F\,v_r/\hbar\omega_L^2$. Eq.s. 6.23 and 6.24 are well known equations in the context of the DC effect in Superconductor Josephson Junctions (SJJ) [45]. In that context $\tilde{I} = I_{ext}/I_c$ where I_{ext} is the external current source and I_c is the critical current. In analogy with the Josephson effect in SJJ, we define

$$I_{ext} = \frac{2F\,I_c}{\hbar\omega_L^2} v_r\ , \tag{6.25}$$

and we will show that I_{ext} can be view as a *dc external "current source"*.

One can easily verify that the quantity

$$G = \frac{1}{2}\omega_L^{-2}\dot{\theta}^2 + V(\theta)\ . \tag{6.26}$$

is a conserved quantity.

6.3.2 Critical velocity

Fig. 6.1 shows the potential $V(\theta)$ for different values of I_{ext} around the critical value I_c. If we consider an arbitrary condition $-\pi < \theta(0) < \pi$, then from the eq.s. 6.23 and 6.24 follows that

1. for $I_{ext} > I_c$ only not periodic and unbounded solutions exist;
2. for $I_{ext} < I_c$ two types of solution exist: (A) periodic and bounded oscillations around some local minimum of the potential 6.24; (B) non periodic and not limited solution;

Not periodic solutions

Not periodic solutions have the asymptotic form for $t \gg 1/\omega_L$

$$\theta(t) \sim \frac{1}{2}\tilde{I}\,\omega_L^2 t^2\ , \tag{6.27}$$

$$z(t) \sim \text{const} + \frac{\hbar}{U_0}\frac{1}{t}\sin\left(\frac{1}{2}\tilde{I}\,\omega_L^2 t^2\right)\ . \tag{6.28}$$

One can see that whereas $\theta(t)$ increases quadratically with t, $z(t)$ has a weak oscillating component with a "frequency" and an amplitude which respectively increases $\left(\sim \tilde{I}\,\omega_L t\right)$ and decreases with time $\left(\propto \frac{1}{t}\right)$.

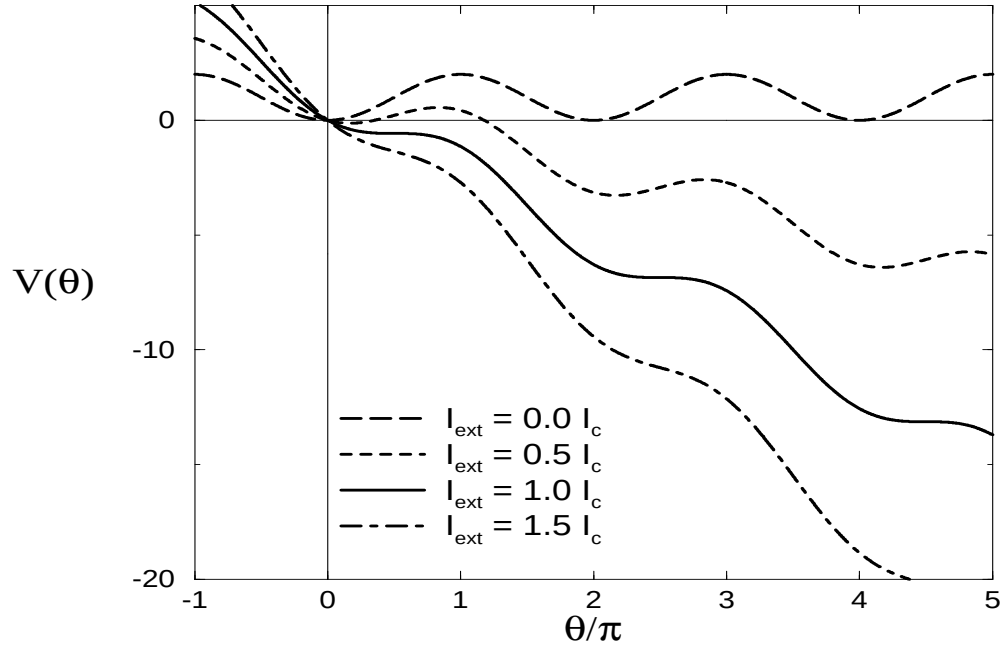

Figure 6.1: Potential energy $V(\theta)$ of the driven weak link BEC at various values of the "external current" I_{ext}.

Periodic solutions

Periodic solutions in the phase θ correspond to a finite time averaged drift in z. In fact, also $\dot{\theta}$ is periodic, and from eq. 6.21 it follows that z must be of the form

$$z = -I_{ext}\, t + z_{oscil} \ . \tag{6.29}$$

The fractional population imbalance z is a sum of a drift term $-I_{ext}\, t$ and a oscillating (and periodic) term z_{oscill}.

Critical velocity

The existence of a critical relative velocity, is simply related to the existence or not of a local minimum in the effective potential $V\,(\theta)$ (see also the fig. 6.1). In particular if $I_{ext} > I_c$ Self-Locking in the population imbalance occurs and we can define a critical velocity v_r^c corresponding to $I_{ext} = I_c$, which is given by

$$v_r^c \equiv \frac{\hbar}{2m}\frac{\omega_L^2}{\omega_0^2}\left(\int d\mathbf{r}\, z\ |\Psi_2|^2\right)^{-1} \ . \tag{6.30}$$

Then if v_r is larger then the critical value v_r^c the adiabatic condition 6.8 breaks and self-locking in the population imbalance occur. If v_r is less then v_r^c the occurrence of self-locking in the population imbalance depends on the initial condition.

6.3.3 Initial conditions

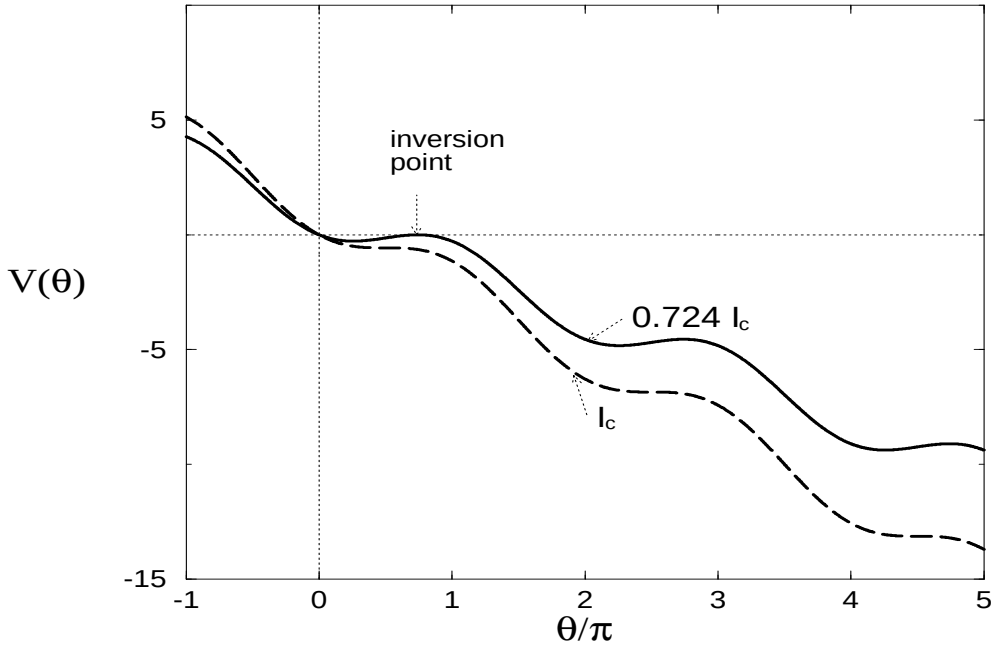

Figure 6.2: Potential energy $V(\theta)$ of the driven Josephson junction at the paricular values of the "external current" $I_{ext} = 0.7246 I_c$ and $I_{ext} = I_c$

Let us consider the case

$$\Delta E\,(t \leq 0) \;=\; 0\;, \tag{6.31}$$

$$\Delta E\,(t > 0) \;=\; 2F\,v_r t\;. \tag{6.32}$$

The conditions under which the system is in equilibrium at $t = 0$ are

$$\theta\,(0) = 0 \quad \text{and} \quad \dot{\theta}\,(0) = 0. \tag{6.33}$$

This is also the case that we will consider later on in the numerical simulation of the proposed experiment. Then the modulus of the velocity can be calculated

starting from the conserved quantity G given by eq. 6.26, with the results

$$\left|\dot{\theta}\right| = \omega_L \sqrt{-2\ \tilde{I}\ \theta - 2\left(1 - \cos\left(\theta\right)\right)}\ . \tag{6.34}$$

We have an inversion point $\theta_0 \neq 0$ if a solution with $\theta \neq 0$ of the equation $\dot{\theta}_0 = 0$ exists. If such inversion point θ_0 exists, then $\theta\left(t\right)$ is a periodic function. θ_0 is a function of the external current I_{ext}. In particular there is a maximal value θ_m as a possible inversion point. This maximal value θ_m is solution of the trascendental eq. $\theta_m \sin\left(\theta_m\right) = 1 - \cos\left(\theta_m\right)$ and takes the value $\theta_m = 2.33112$ ($\sin\left(\theta_m\right) = 0.724613$). Correspondingly, we have a maximal value $I_{ext}^{\max}$of the "external current source" I_{ext} (or a maximal value v_r^m of the laser drift velocity v_r)

$$I_{ext}^{\max} = \sin\left(\theta_m\right) I_c\ , \tag{6.35}$$

and

$$v_r^m = \sin\left(\theta_m\right) \frac{\hbar}{2m} \frac{\omega_L^2}{\omega_0^2} \left(\int d\mathbf{r}\ z\ \left|\Psi_2\right|^2\right)^{-1}\ , \tag{6.36}$$

and

$$z\left(v_r^m\right) = 2 \sin\left(\theta_m\right)\ I_c\, t_f\ . \tag{6.37}$$

From the experimental determination of the critical value of v_r^m and of the maximum $z\left(v_r^m\right)$ value of z, the relevant quantity ω_L and I_c can be indirectly[10] determined through

$$\omega_L = \omega_0 \sqrt{\frac{v_r^m}{\sin\left(\theta_m\right)} \frac{2m}{\hbar} \int d\mathbf{r}\ z\ \left|\Psi_2\right|^2}\ , \tag{6.38}$$

and

$$I_c = \frac{1}{2\sin\left(\theta_m\right)} \frac{z\left(v_r^m\right)}{t_f}\ . \tag{6.39}$$

Fig. 6.2 shows the potential $V\left(\theta\right)$ corresponding to this particular value of the external current $I_{ext}^{\max} = 0.7246\, I_c$. From this figure it is also clear that with the boundary condition $\theta\left(0\right) = 0$ and $\dot{\theta}\left(0\right) = 0$ we have that

1. for $I_{ext} > \sin\left(\theta_m\right) I_c$ the solution $\theta\left(t\right)$ is not periodic and unbounded;

2. for $I_{ext} < \sin\left(\theta_m\right) I_c$ the solution $\theta\left(t\right)$ is periodic and bounded;

[10] also through the determination of the integral $\left(\int d\mathbf{r}\ z\ \left|\Psi_2\right|^2\right)$.

6.3.4 Brief summary

Depending on the initial condition we can have bound solutions around a local minimum that correspond to a drift in the population imbalance $z(t)$. If we have as initial condition $\theta(0) = 0$ and $\dot{\theta}(0) = 0$ we have a maximal value of the laser drift velocity $v_r^m \simeq 0.7246\, v_r^c$ and in the small velocity limit $|v_r| \ll v_r^c$ we have the simple analytical solution for the population imbalance $z(t) = E_J \frac{v_r}{v_r^c}\left(t - \frac{1}{\omega_L}\sin(\omega_L t)\right)$.

6.4 Adiabatic condition on the effective TMA

In chapter 5 we have shown that the numerical integrations of the Gross-Pitaevskii equation (GPE) in a double well potential indicates that the low energy tunneling dynamics can be accurately described by an effective TMA. Also in this case, in which the external potential $V_{ext}(\mathbf{r}, t)$ is time dependent, we may give an effective description

$$\hbar\,\dot{z} = -2E_J^*\sqrt{1-z^2}\sin(\theta)\,, \tag{6.40}$$

$$\hbar\,\dot{\theta} = \Delta E^*(t) + 2E_J^*\frac{z}{\sqrt{1-z^2}}\cos(\theta) + U_0^*\,z\,, \tag{6.41}$$

in the form of the variational TMA eq.s. 6.20 and 6.21, in which the relevant physical quantities U_0^*, E_J^*, $\Delta E^*(t)$ are a "phenomenological" input. We recall that from the numerical integrations of the GPE, we can determine directly the Josephson frequency ω_L and the critical current I_c. The effective equations of motion are obtained by substituting the Josephson coupling energy $E_J = (h + U_3)$ (eq. **??**) and the mean field integral U_0 (defined in eq. 4.7) with

$$E_J^* = \hbar I_c\,, \tag{6.42}$$

$$U_0^* = \frac{\hbar\omega_L^2}{2I_c}\,. \tag{6.43}$$

With these substitutions we have obtained the excellent results for the time independent external potential case showed in section 5.5. Now the problem: which is the way to define the effective "zero point energy" $\Delta E^*(t)$? In the case in which $\Delta E^*(t)$ changes slowly in time we can give the following answer.

Adiabatic condition

Assuming $U_0^* \gg \hbar I_c$, the equations of motion 6.40 and 6.41 read

$$\hbar \dot{z} = -2E_J^* \sqrt{1-z^2} \sin(\theta) \ , \tag{6.44}$$

$$\hbar \dot{\theta} = \Delta E^*(t) + U_0^* \ z \ . \tag{6.45}$$

If $\Delta E^*(t)$ changes sufficiently slowly in time $\dot{\theta}(t) \approx 0$ and $z(t) \approx -\Delta E^*(t)/U_0^*$. On the other hand, within the validity of eq. 6.8 $z(t)$ must correspond to the equilibrium value $\langle z \rangle_{eq}$ at the time t. Then the effective "zero point energy" $\Delta E^*(t)$ can be estimated by

$$\Delta E^*(t) = -U_0^* \ \langle z \rangle_{eq} \, , \tag{6.46}$$

where $\langle z \rangle_{eq}$ can be determined by solving eq. 6.8. In the case in which the laser barrier moves with constant velocity (in the small velocity limit) we obtain from 6.46 that

$$\Delta E^*(t) = 2F^* v_r t \ , \tag{6.47}$$

$$F^* = -\frac{1}{2} U_0^* \frac{\partial \langle z \rangle_{eq}}{\partial a} \, , \tag{6.48}$$

where $a = v_r \, t$ is the position of the laser barrier. Furthermore $\frac{\partial \langle z \rangle_{eq}}{\partial a}$ can be also calculated in the framework of the time independent linear response theory[11].

Validity limit

We have implicitly assumed that the displacement of the potential is sufficiently small to use constant values of the Josephson frequency and critical current.

[11] For a small displacement da of the laser the variation in the external potential is $\delta V_{ext} = \frac{\partial V_{laser}}{\partial a} da$. The variation

$$\delta\Psi = \left(H_0 - \mu_0 + 3g \left| \Psi_0 \right|^2 \right)^{-1} \left(\delta V_{ext} - \delta\mu \right) \ \Psi_0 \ ,$$

where $\delta\mu$ is the chemical potential variation. The constraint on the conservation of the norm implies

$$\delta\mu = \int \rho_0 \ \left(\delta V_{ext} + g\delta\rho \right) \ .$$

(in the symmetric double well potential $\delta\mu$ is, for symmetry reasons, zero). The variation of the fractional population imbalance δz is by definition a simple function of the variation in the density $\delta\rho$, that is related with the variation in the ground state wave function $\delta\Psi$ through $\delta\rho = 2\Psi_0 \delta\Psi$.

6.5 Conclusion

We have explained that a moving laser in the trap improves the observability of the Josephson-like effects in the BEC weak-link. In particular we have found a practical method to obtain an indirect measure of ω_L and I_c through the experimental determinations of the critical value of the relative velocity v_r^m and the maximum value of the function $z\left(v_r\right)$ for $v_r \approx v_r^m$. We rewrite here the important eq.s 6.38 and 6.39

$$\omega_L = \omega_0 \sqrt{\frac{v_r^m}{\sin\left(\theta_m\right)} \frac{2m}{\hbar} \int d\mathbf{r}\, z \, \left|\Psi_2\right|^2}\,, \tag{6.49}$$

$$I_c = \frac{1}{2\sin\left(\theta_m\right)} \frac{z\left(v_r^m\right)}{t_f}\,, \tag{6.50}$$

where as shown in subsection $6.3.3$, the numerical factor $\sin\left(\theta_m\right)$ comes out from the initial conditions defined in eq.s 6.31, 6.32 and 6.33. Then the presence of fluctuations of the population imbalance (Josephson "plasma" oscillations), due to these initial conditions, reduces the values of the critical velocity and the maximum value of the function $z\left(v_r\right)$. This is also expressed by eq.s 6.36 and 6.37, that we also rewrite for clarity in the following

$$v_r^m = \sin\left(\theta_m\right) \frac{\hbar}{2m} \frac{\omega_L^2}{\omega_0^2} \left(\int d\mathbf{r}\, z \, \left|\Psi_2\right|^2 \right)^{-1}\,, \tag{6.51}$$

$$z\left(v_r^m\right) = 2\sin\left(\theta_m\right)\, I_c\, t_f \quad . \tag{6.52}$$

Furthermore, in the case in which Josephson oscillations are strongly damped (in a time scale shorter than $1/\omega_L$), and therefore difficult to directly observed, the DC component of the current is preserved, and the factor $\sin\left(\theta_m\right)$ can be neglected. It follows that the possibility to detect experimentally the Josephson effect is not at all reduced (at contrary it is a little improved).

Eq. 6.51 is of practical utility for the precise determination of trap and laser parameters.

Chapter 7

..numerical results

In this chapter we show the results obtained by solving numerically the GPE for the experiment proposed in the chapter 6 and compare them with those obtained with an effective TMA. In section 2, we consider a detailed analysis based on the numerical integration of the standard time dependent GPE in a realistic 3D trapping potential, referred to the JILA setup [8]. A similar analysis for the MIT setup is in progress. The numerical results demonstrate that also in the case of a time-dependent Hamiltonian, an effective TMA can be used to describe the low energy dynamical behaviour of the two wells system. It is also shown that it is possible to give an indirect measure of the "plasma" frequency ω_L and the critical current I_c. We will discuss in a subsection an interesting resonance effect between the longitudinal intrawell dipole mode and the tunneling dynamics, that cannot be described in terms of the effective TMA. In the following subsection we show (as a check) that the effective parameters of the TMA have only a weak dependence on the laser position.

7.1 The proposed experiment for the JILA setup

We have considered the JILA setup with $N = 50.000$ Rb atoms where a thin laser barrier cuts the condensate in "two" parts. The harmonic trap is cylindrically symmetric, with a longitudinal frequency ω_0 of 50.0 Hz and a radial frequency ω_r of 17.68 Hz. We have used as scattering length the value $a = 58.19$ Angstrom (the more precise actual value is $a = 57.7$ Angstrom [47]). Using the longitudinal harmonic oscillator as natural scale of dimensions and energy, we obtain an adimensional coupling constant $g^{adim} = 2396.2$. With this adimensional scales, the units length scale is $l_0 = 1.5256$ μm, and the unit time scale is $\omega_0^{-1} = 3.1831$ ms. A laser sheet (of longitudinal gaussian shape) is focused in the center of the trap. We assume that the longitudinal $1/e^2$ half-width of the laser barrier is 3.5 μm. The laser height used is $13\,\hbar\omega_0$. We have used a grid of 84×77 where 84 (77) is the number of longitudinal (radial) discretization points. This grid leads to an accuracy of $\sim 1\%$ on the critical current I_c and on the Josephson plasma frequency ω_L.

The starting point of our numerical analysis has been to find (using the self consistent variational TMA discussed in the previous chapter) a good set of physical parameters, to achieve a good compromise between different experimental needs, such as the choice of time scale, the dimension scale of the condensate, and laser sheet parameters. We have first estimated ω_L and I_c, and subsequently the critical population imbalance z_c. Then we have computed the exact value of ω_L, by solving numerically GPE with an initial imbalance $z \ll z_c$. Once the exact value z_c is found, the current-phase relations is obtained starting from an initial imbalance $z \sim z_c$. From this relation the critical current I_c is finally determined[1].

We report in the following the results about the numerical simulation of the proposed experiment. The population imbalance is "measured" after the time $t_f = 1\ s$. This time was chosen requiring that $z\left(t = t_f\right)$ is of the order ~ 0.4 (value that is clearly observable). The fig. 7.1 shows the results for z at $t = 1s$, versus different values of the laser velocity v_r. Crosses are calculated with the full numerical integration of the GPE and the solid line corresponds to the effective TMA.

[1]The exact value of I_c is in good agreement with that obtained in the SCVTMA (within an accuracy of $\sim 1\%$).

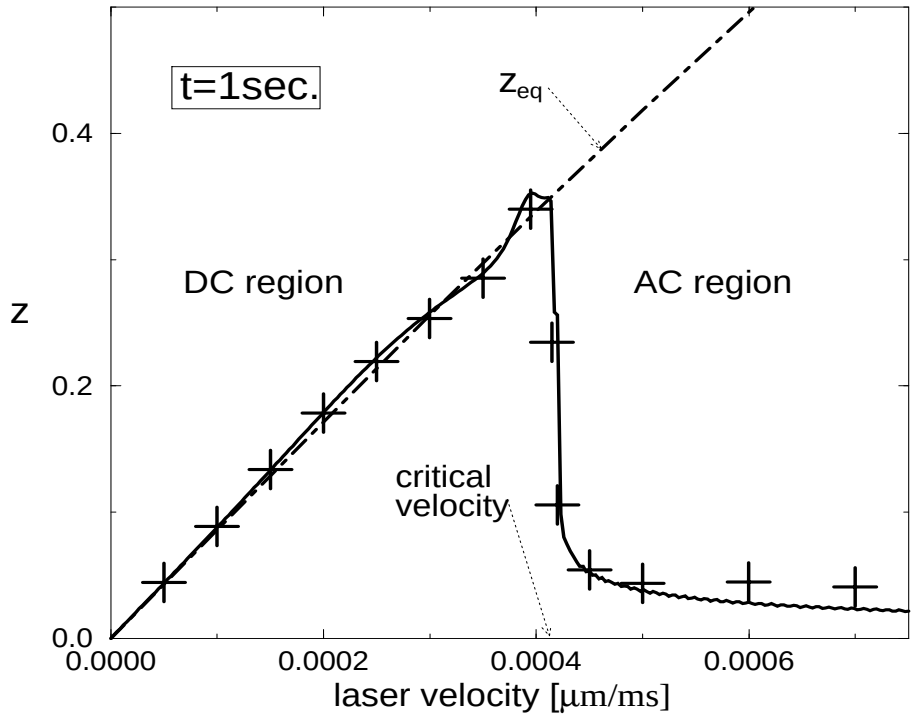

Figure 7.1: JILA setup: numerical results evidentiate a critical behaviour of the population imbalance. z is calculated after $1\ s$ versus different laser velocities. Crosses and solid line correspond to the results of the GPE and of the effective TMA, respectively. Dashed line represents the equilibrium value z_{eq} in the "final" position $v_r\, t_f$ of the laser barrier (time independent GPE). Note that for $v_r > 0.00042\ \mu m/ms$ the differences between the numerical results for z and the equilibrium values z_{eq} become immediately very large.

Analyzing the population imbalance versus v_r, a critical behaviour appears. Such effects manifest itself in a jump of the curve $z\,(v_r)$ in correspondence to the value $v_r \approx 0.00042\ \mu m$. This critical value agrees well with the value v_r^m estimated with eq. 6.36. Also the maximum of the curve $z\,(v_r) \approx 0.35$ agrees well with the value $z\,(v_r^m)$ of eq. 6.37. Therefore using the numerical results $v_r \approx 0.00042\ \mu m$ and $z\,(v_r) \approx 0.35$ one can verify that both I_c given in eq. 6.39and ω_L given in eq. 6.38 can be indirectly measured with a relative error of few $\%$.

Dashed line (fig. 7.1) represents the equilibrium values z_{eq} of z calculated with the eq. 6.8 (stationary GPE) when the laser barrier is in the "final" position

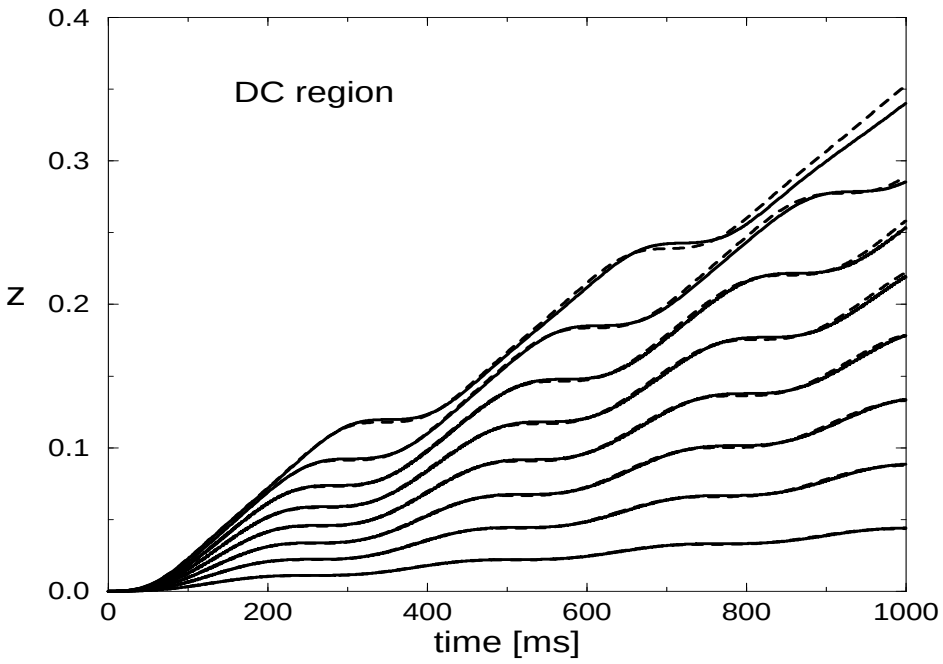

Figure 7.2: JILA setup: $v_r < v_r^m$. Fractional population imbalances evolution $z\,(t)$ for $0 < t < t_f = 1\,\mathrm{sec}$ for the velocity values of the first eight crosses of the fig. 7.1, below the critical velocity. Solid line is the numerical integration of the GPE and long dashed line correspond to the effective TMA. $z\,(t)$ decomposes exactly in a DC component $dz\,(t)\,/dt \approx I_{ext}$ and an oscillating part. The DC component of $z\,(t)$ increases both with the time and velocity v_r.

$v_r \cdot t_f$ (along the z-axis). Note that for $v_r < v_r^m$ the numerical results for z agree well with the equilibrium values z_{eq} and for $v_r > v_r^m$ the difference between the numerical results for z and the equilibrium values z_{eq} become immediately very large. We have observed two separate regions, which can be called the "DC" and the "AC" regions, because of the formal similarity of the eq.s. 6.23 and 6.24 with the SJJ equations in the presence of a dc current source.

- for $v_r < v_r^m$ we have a "DC" region, namely a DC supercurrent flow of atoms between the two wells (or superconducting region). The flow of atoms is approximately proportional to the time t_f and $z \sim z_{eq}$. (see also fig. 7.2)

- for $v_r > v_r^m$ we have an "AC" region. In this region a difference in the

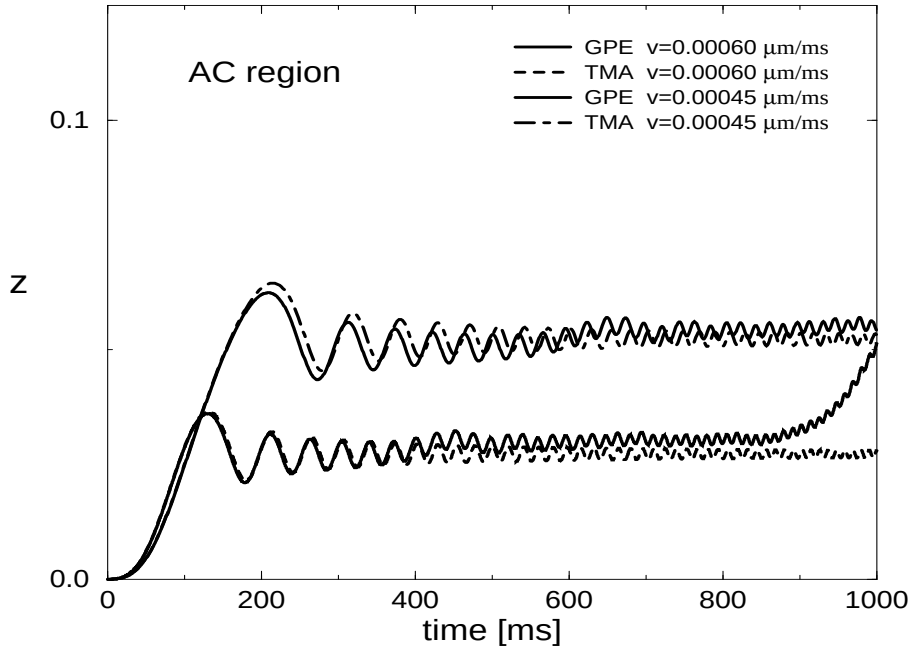

Figure 7.3: JILA setup: $v_r > v_r^m$. Fractional population imbalance evolution for $0 < t < 1s$ with velocity values corresponding to the 11th and 13th cross of fig. 7.1. Note the agreement for the frequency of the AC oscillations between effective TMA calculations and GPE. The first small deviations appear as the frequency reaches that of the lowest radial intrawell mode: a small resonance effect appear. In the case $v = 0.00060\ \mu m/ms$ we have for $t > 900\ ms$ a strong resonance effect between the dipole intrawell mode.

chemical potential occurs (Self Trapped or insulator region). The supercurrent oscillates at a frequency approximately proportional to $z - z_{eq}$ and increases with the time t_f.

Let us discuss separately the "DC" region $v_r < v_r^m$, the "AC" region $v_r > v_r^m$ and the transition region $v_r \approx v_r^m$. For each of these regions we show the time evolution $z\,(t)$ for $0 < t < t_f = 1\,\mathrm{sec}$.

In fig. 7.2 we show for $v_r < v_r^m$ the fractional population imbalance $z\,(t)$ evolution for the values of the laser velocity v_r corresponding to the first eighth crosses of fig. 7.1. For small displacement of the laser $v_r t_f$ and for velocity smaller than the critical velocity the agreement between GPE (solid line) and effective TMA (dotted line) is extremely good. The evolution $z\,(t)$ consists of

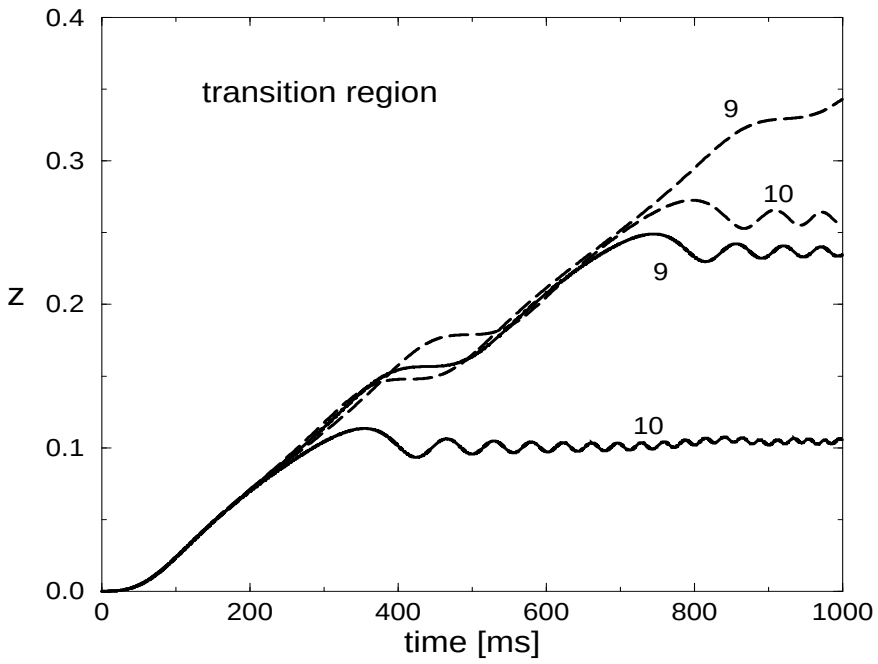

Figure 7.4: JILA setup: $v_r \approx v_r^m$. Fractional population imbalance evolution during $1s$ with velocity values correspondingly to the 9th and 10th cross of fig. 7.1. Solid line is the numerical integration of the GPE and long dashed line corresponds to the effective TMA.Solid line is the numerical integration of the GPE and long dashed line corresponds to the effective TMA. For laser velocity near its critical value v_r^m the effective TMA cannot fit well the numerical results, because of the sharp incline of the curve $z\left(v_r\right)$ in fig. 7.1. In fact a small error in v_r causes a large indetermination in z.

a mean atom flux through the barrier proportional to I_{ext} (DC regime), plus a Josephson plasma oscillation with amplitude and frequency depending on the laser velocity[2]. The Josephson oscillations are due to the fact that we start to move the laser abruptly at $t = 0$ with the constant value v_r for $t > 0$. If the velocity v_r is reached in a time large compared to $1/\omega_L$, the DC component is the only appreciable.

In conclusion, although Josephson oscillations can be difficult to observe, the mean average of the population imbalance is observable and the occurrence of a sudden jump in $z\left(t_f, v_r\right)$ as a function of v_r, will be a clear evidence of Josephson-like effects in a BEC Weak-Link.

[2]more in general they must depend also on the initial conditions.

In fig. 7.3 we show the evolution $z\,(t)$ for $0 < t < t_f = 1\,\mathrm{sec}$ for $v_r > v_r^m$ corresponding to the 11th and 13th crosses of the fig. 7.1. The numerical results (solid line) show a small deviations from the effective TMA (dotted line); a brief discussion of such deviations is given in the following subsection.

In fig. 7.4 we show the evolution $z\,(t)$ for $0 < t < t_f = 1\,\mathrm{sec}$ for $v_r \approx v_r^m$ corresponding to the 9th and 10th crosses of fig. 7.1. Solid line is the numerical integration of the GPE and long dashed line corresponds to the effective TMA. For laser velocity near its critical value v_r^m the effective TMA cannot fit well the numerical results, because of the jump of the curve $z\,(v_r)$ (see fig. 7.1). In fact a small error in v_r causes a large indetermination in z.

7.1.1 Breakdown of the effective TMA and resonance effects

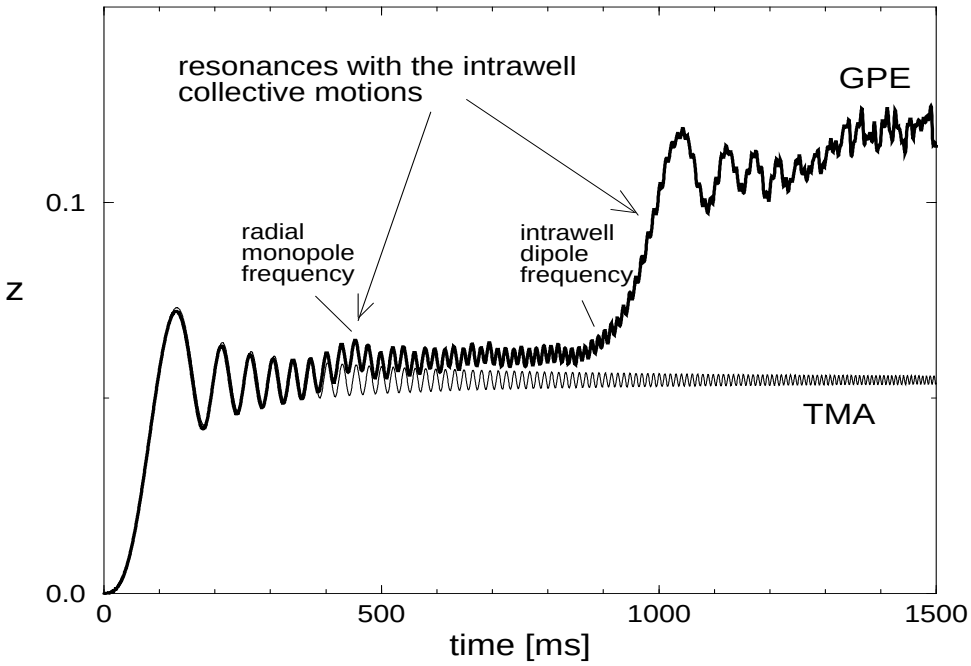

Figure 7.5: JILA setup: fractional population imbalance evolution $z\,(t)$ for $0 < t < 1900$ ms with the velocity that correspond to the 13th cross of fig. 7.1. Solid line is the numerical integration of the GPE and thin line correspond to the effective TMA.

Non trivial dynamical behaviour can take place because of the coupling between intrawell motions and interwell dynamics, when the Josephson frequency in the

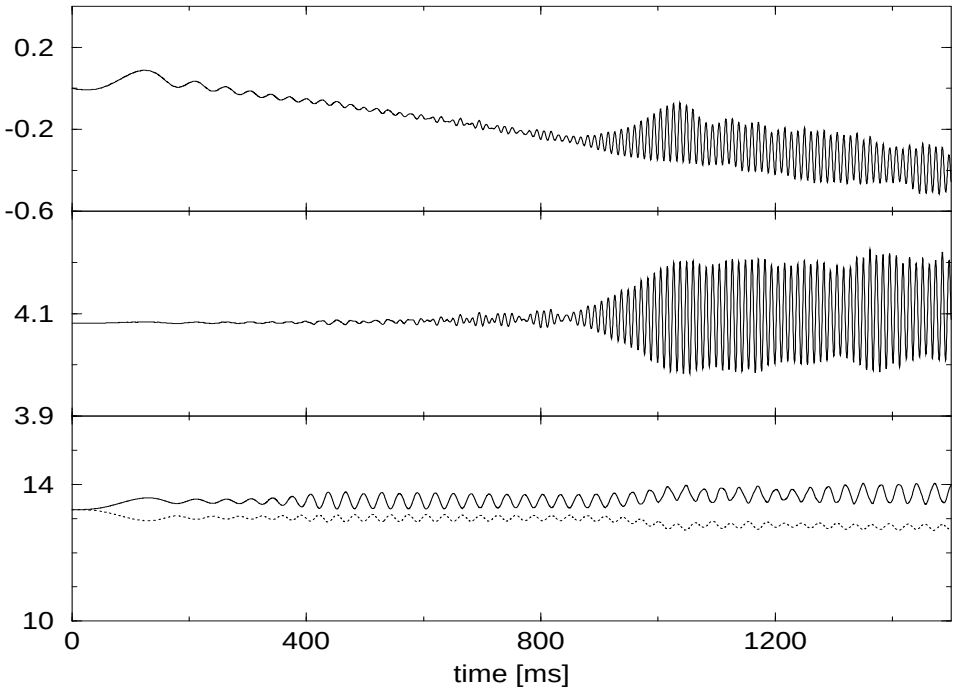

Figure 7.6: JILA setup: Top: dipole moment. Middle: longitudinal monopole moment. Bottom: solid (dotted) line correspond to the right (left) well radial monopole moment. These data correspond to the same calculation of previous fig. 7.5

self trapping regime (AC-like) is comparable to the frequency of some intrawell mode. In fig. 7.5 we display, as an example, the fractional population evolution $z(t)$ for $0 < t < 1900\,ms$ in correspondence to the laser velocity of the 13th cross of fig. 7.1 ($v_r \sim 0.0006$ μm/ms). Notice that the frequency of Josephson oscillations increases in time in accord with the effective TMA for $t < 900\ ms$. When this frequency becomes comparable with the longitudinal dipole intrawell frequency ($\sim \omega_0$), the population of the second well changes to another value (approximately the double of the TMA prediction).

This effect can be qualitatively understood by using an effective three level system model, in which in addition to the left and right states, Ψ_1 and Ψ_2, an effective dipole mode Ψ_2^d is included on the right well. The effective TMA equations, expressed in terms of the amplitudes c_1 and c_2 can be written as

$$i\,\hbar\frac{\partial}{\partial t}\begin{pmatrix} c_1 \\ c_2 \end{pmatrix} = \begin{pmatrix} U_0^*|c_1|^2 + \Delta E^*(t) & E_J^* \\ E_J^* & U_0^*|c_2|^2 \end{pmatrix}\begin{pmatrix} c_1 \\ c_2 \end{pmatrix}. \qquad (7.1)$$

If one includes the dipole mode, the equations become

$$i\,\hbar\frac{\partial}{\partial t}\begin{pmatrix} c_1 \\ c_2 \\ c_2^d \end{pmatrix} = \begin{pmatrix} U_0^*|c_1|^2 + \Delta E^*(t) & E_J^* & E_{Jd}^* \\ E_J^* & U_0^*|c_2|^2 & 0 \\ E_{Jd}^* & 0 & U_{0d}^*|c_2^d|^2 + \omega_d \end{pmatrix}\begin{pmatrix} c_1 \\ c_2 \\ c_2^d \end{pmatrix} \quad (7.2)$$

where c_2^d is the amplitude corresponding to Ψ_2^d, $\omega_d \sim \omega_0$ is the dipole frequency, U_{0d}^* is an effective capacitive energy (referred to the occupation of the dipole mode Ψ_2^d) and E_{Jd}^* is an effective off-diagonal term between Ψ_1 and Ψ_2^d. This equations is able to explain qualitatively the jump in population observed in 7.1 after $900\ ms$ if $U_{0d}^* \approx U_0^*$ and $E_{Jd}^* \approx E_J^*$. In fact, in that case, after some time, the system occupies the Ψ_2^d state. This explains the jump in the population of the second well, and the amplitude of the jump is comparable to the TMA prediction. When this transition occurs, dipole oscillations of amplitude proportional to $\mathrm{Re}\left(c_2^* c_2^d \langle\Psi_1|\, z\, |\Psi_2^d\rangle\right)$ can be observed.

While it is not difficult to understand why $U_{02}^* \approx U_0^*$ (these are bulk terms), we don't have any microscopic explanation of the reason why E_{J2}^* should be almost equal to E_J^*.

Fig. 7.6 provides more direct information about this feature. The intrawell dipole mode manifests both in the dipole moment

$$d_1 = \int d\mathbf{r}\, z\, |\Psi|^2\,, \quad (7.3)$$

and in the longitudinal monopole moment

$$m_z = \int d\mathbf{r}\, z^2\, |\Psi|^2\,. \quad (7.4)$$

Direct integration of the GPE shows that also the low energy radial monopole mode is excited, as it can be seen from the radial monopole moment

$$m_r = \int d\mathbf{r}\, \left(x^2 + y^2\right)\, |\Psi|^2 \quad (7.5)$$

shown in fig. 7.6. Note that the effect is smaller than in the case regarding the dipole mode.

7.1.2 *A test on the effective parameters

A more sophisticate description of the moving laser dynamics as that provided by the effective TMA introduced in section 6.3, requires the use of effective

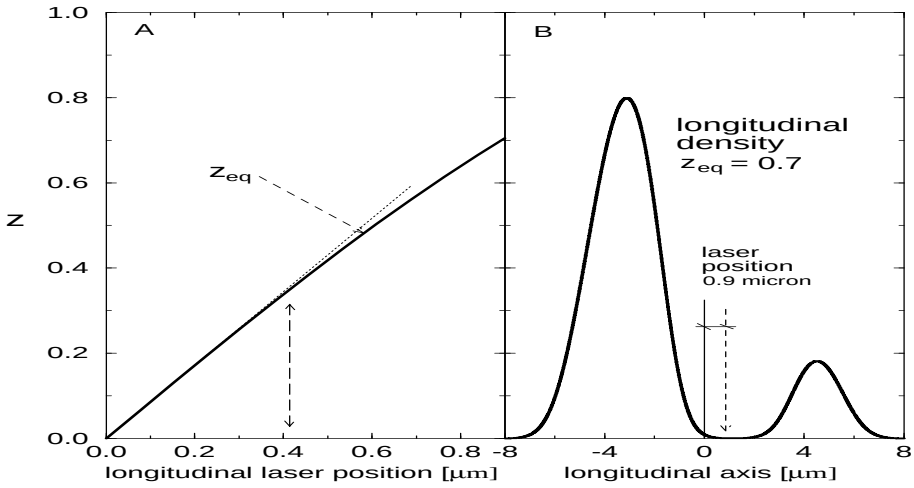

Figure 7.7: (A): equilibrium value of z versus the laser position a. (B): longitudinal equilibrium density for the maximum displacement of the laser considered in the simulation $a = 0.9\ \mu m$.

energy parameters which depend on the laser position a

$$U_0^* = U_0^*(a)\,,\ E_J^* = E_J^*(a) \text{ and } \Delta E^* = \Delta E^*(a)\ . \tag{7.6}$$

Such functions must be calculated to reproduce within the effective TMA, the GPE numerical results at each laser position a. This approximation has not been considered here in a detailed way and it is beyond the scope of the present work. We limit to observe that, for symmetry reasons, one gets the relations

$$\frac{\partial(U_0^*)}{\partial a}|_{a=0} = 0\,,\ \frac{\partial(E_J^*)}{\partial a}|_{a=0} = 0\ , \tag{7.7}$$

$$\frac{\partial(\Delta E^*)}{\partial a}|_{a=0} = 2F \text{ and } \frac{\partial(\Delta E^*)}{\partial^2 a}|_{a=0} = 0\,. \tag{7.8}$$

We have checked that $\frac{\partial(U_0^*)}{\partial^2 a}|_{a=0}$, $\frac{\partial(E_J^*)}{\partial^2 a}|_{a=0}$ give negligible corrections for our purpose, and most of the discrepancy comes out from the coupling with others collective motions. We have checked that the values of the most relevant physical quantities are all almost independent on the laser position in the region of interest $0 < a < 0.4\,\mu m$ (values that correspond to the region $0 < v_r < v_r^m$ in fig. 7.1).

Fig. 7.7 A shows the equilibrium values of fractional population imbalance $z_{eq}(a)$ versus the laser position a. In our effective TMA we have linearized $z_{eq}(a) \approx \frac{\partial(z_{eq})}{\partial a}|_{a=0}\ a$. Fig. 7.7 B shows the equilibrium longitudinal density

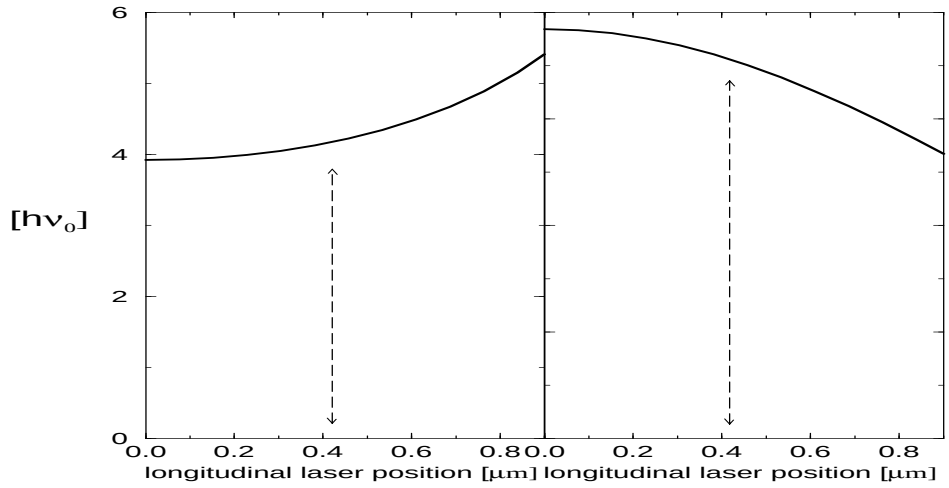

Figure 7.8: Left: U_0^* versus the laser position a. Right: normalized critical current $\frac{I_c}{\sqrt{1-z_{eq}^2}}$ versus the laser position a.

profile calculated at the maximum value of the laser displacement considered $a = 0.9\,\mu m$. Note that, despite of the fact that a is less then $1\mu m$ and the longitudinal extent of the condensates is about $6\ \mu m$, the fractional population equilibrium imbalance is higher then 0.7.

Fig. 7.8 A shows the value of U_0^* versus the laser position a. Fig. 7.8 B shows the value E_J^* normalized by the factor $\sqrt{1-\langle z\rangle_{eq}^2}$. In the region of interest the effective energy integrals U_0^* and E_J^* change only of 5%.

7.2 Summary

The numerical results (GPE) demonstrate that the low energy tunneling dynamics can be accurately described by an effective TMA, also in the case in which the external potential is time dependent. The non-linear dynamical behaviour of the two weakly coupled BECs can be described in terms of a macroscopic quantum phase-difference θ and in terms of the fractional population difference z between the two sub-systems. We have showed that the relevant variables θ and z satisfy a non linear equation depending parametrically only through tree energy terms: the Josephson frequency ω_L, the critical current I_c, and the difference in the "zero point energy" $\Delta E\,(t)$ (or equivalently through the average force F).

Bibliography

[1] M. H. Anderson, J. R. Ensher, M. R. Matthews, C. E. Wieman and E. A. Cornell, Science **269**, 198 (1995).

[2] C. C. Bradley, C. A. Sackett, J. J. Tollett, and R. G. Hulet, Phys. Rev. Lett. **75**, 1687 (1995).

[3] K. B. Davies, M. O. Mewes, M. R. Andrews, N. J. van Druten, D. S. Durfee, D. M. Kurn, and W. Ketterle, Phys. Rev. Lett. **75**, 3969 (1995).

[4] M. O. Mewes, M. R. Andrews, N. J. van Druten, D. M. Kurn, D. S. Durfee, C. G. Townsend and W. Ketterle, Phys. Rev. Lett. **77**, 416 (1996); **77**, 988 (1996).

[5] J. R. Ensher, D. S. Jin, M. R. Mattews, C. E. Wieman, and E. A. Cornell, Phys. Rev. Lett. **77**, 4984 (1996).

[6] Cornell, E., J. Res. Natl. Stand. Technol. **101**, 419 (1996).

[7] M. R. Andrews, C. G. Townsend, H.-J. Miesner, D. S. Durfee, D. M. Kurn, and W. Ketterle, *Observation of Interference Between Two Bose Condensates*, Science **275**, 637 (1997).

[8] D. S. Hall, M. R. Mattews, C. E. Wieman, and E. A. Cornell, *Measurements of Relative Phase in Binary Mixtures of Bose-Einstein Condensates* cond-mat/9805327.

[9] M. R. Andrews, D. M. Kurn, H.-J. Miesner, D. S. Durfee, C. G. Townsend, S. Inouye, and W. Ketterle, *Propagation of Sound in a Bose-Einstein Condensate*, Phys. Rev. Lett. **79**, 553 (1997).

[10] B. D. Josephson Phys. Lett. **1**, 251 (1962).

[11] P. W. Anderson, in *The Lesson of Quantum Theory*, J. D. Boer, E. Dal, O. Ulfbeck, Eds. (Elsevier, Amsterdam, 1986), pp. 23-33.

[12] R. Feynman, *The Feynman lectures on Physics*, (Addison-Wesley Publ. Comp., 1965).

[13] O. Avenel, and E. Varoquaux, Phys. Rev. Lett. **55**, 2704 (1985).

[14] S. V. Pereverzev, A. Loshak, S. Backhaus, J. C. Davis, and R. E. Packard, *Quantum oscillations between two weakly coupled reservoirs of superfluid* ^{3}He-B, Nature **388**, 449 (1997).

[15] S. Backhaus, S. V. Pereverzev, A. Loshak, J. C. Davis, R. E. Packard, *Direct Measurement of the Current-Phase Relation of a Superfluid* ^{3}He-B *Weak Link*, Science **278**, 1435 (1997).

[16] F. Dalfovo, L. Pitaevskii, and S. Stringari, *Order parameter at the boundary of a trapped Bose gas*, Phys. Rev. A **54**, 4213 (1996).

[17] A. Smerzi, S. Fantoni, S. Giovanazzi, and S. R. Shenoy, *Quantum Coherent Atomic Tunneling between Two Bose-Einstein Condensates*, Phys. Rev. Lett. **79**, 4950 (1997).

[18] S. Raghavan, A. Smerzi, S. Fantoni, and S. R. Shenoy, *Coherent Tunneling of Bose-Einstein Condensates: Exact Solutions for Josephson Effects and Macroscopic Quantum Self-Trapping*, preprint cond-mat/9706220.

[19] I. Zapata, F. Sols, and A. Leggett, *Josephson effect between trapped Bose-Einstein condensates* cond-mat/9707143.

[20] G. J. Milburn, J. Corney, E. M. Wright, and D. F. Walls, *Quantum dynamics of an atomic Bose-Einstein condensate in a double-well potential*, Phys. Rev. B **55**, 4318 (1997).

[21] M. J. Steel, and M. J. Collett, *Quantum state of two trapped Bose-Einstein condensates with a Josephson coupling*, cond-mat/9710124.

[22] J. Williams, R. Walser, J. Cooper, E. Cornell, and M. Holland *Nonlinear Josephson-type oscillations of a driven, two-component Bose-Einstein condensate* cond-mat/9806337.

[23] V. L. Ginzburg and L. P. Pitaevskii, Zh. Eksp. Teor. Fiz. **34**, 1240 (1958), Sov. Phys. JEPT **7**, 858 (1958); E. P. Gross, Nuovo Cimento **20**, 451 (1961); J. Math. Phys. **46**, 137 (1963).

[24] S. Backhaus, S. V. Pereverzev, R. W. Simmonds, A. Loshak, J. C. Davis, and R. E. Packard, *Discovery of a metastable π-state in a superfluid ^{3}He weak link*, Nature **392**, 687 (1998).

[25] S. Giovanazzi, A. Smerzi, and S. Fantoni, *(in progress)*.

[26] S. Giovanazzi, and S. Fantoni, *(in progress)*.

[27] A. Griffin, D. W. Snoke and S. Stringari, *Bose Einstein Condensation*, (Cambridge Univ. Press, Cambridge, 1995).

[28] P. Nozieres, and D. Pines, *The Theory of Quantum Liquids, vol 2: Superfluid Bose Liquids*, (Addison-Weley Publishing Co., 1990).

[29] P. Sokol, in [36].

[30] S. Moroni, G. Senatore, and S. Fantoni, Phys. Rev. B. **55**, 1040 (1997); S. Moroni, S. Fantoni, and A. Fabrocini, in press.

[31] J.P. Wolfe, J.L. Lin, and D.W.Snoke, in [36].

[32] W. D. Phillips, Rev. Mod. Phys., in press.

[33] N. N. Bogoliubov, J. Exptl. Theoret. Phys. (USSR) **34**, 58 (1958); translation: Soviet Phys. JETP **7** 41 (1958).

[34] A. L. Fetter, *Ground state and excited states of a confined condensed Bose gas*, Phys. Rev. B **53**, 4245 (1996).

[35] S. Stringari, *Collective Excitations of a Trapped Bose-Condensed Gas* Phys. Rev. Lett. **77**, 2360 (1996).

[36] A. Griffin, *Excitations in a Bose-Condensed Liquid*, (Cambridge Univ. Press, Cambridge, 1993).

[37] C. W. Gardiner, *Particle-number-conservig Bogoliubov meth....*, Phys. Rev. B **56**, 1414 (1997).

[38] V. M. Perez-Garcia, H. Michinel, J. I. Cirac, M. Lewenstein, and P. Zoller, *Low Energy Excitations of a Bose-Einstein Condensate: A Time-Dependent Variational Analysis* Phys. Rev. Lett. **77**, 5320 (1996).

[39] R. L. Pfleegor and L. Mandel, Phys. Rev. **159**, 1084 (1967).

[40] P. A. M. Dirac, *Quantum Mechanics*, (Oxford Univ. Press, London, 1958), 4th ed., Chap. 1, p. 9.

[41] P. A. M. Dirac, Proc. Cambridge Philos. Soc. **26**, 376 (1930). See also, F. Cooper, S.-Y. Pi, and P. Stancioff, Phys. Rev. D **34**, 3831 (1986), and reference therein.

[42] F. Cooper, J. Dawson, S. Habib, and R. D. Ryne, submited.

[43] A. Das, *Integrable Models, Lecture Notes in Physics*, 30 (Word Scientific, Singapore, 1989).

[44] B. Yoon, and J. W. Negele, *Time-dependent Hartree approximation* .. Phys. Rev. A **16**, 1451 (1977).

[45] K. K. Likharev, *Dynamics of Josephson Junctions and Circuits*, 66 (1986).

[46] U. Leonhardt, T. Kiss, and P. Piwnicki *Quantum backaction of optical observations on Bose-Einstein condensates*, quant-ph/9801048.

[47] H. M. J. M. Boesten, C. C. Tsai, J. R. Gardner, D. J. Heinzen, and B. J. Verhaar, Phys. Rev. A **55**, 636 (1997).